Effect of magnetic field on vibration of electrorheological fluid nanoplates with FG-CNTRC layers

Peyman Roodgar Saffari [a,] *, Sikiru Oluwarotimi Ismail [b,] * ,Chanachai Thongchom [a,] *,Sayan Sirimontree [a] , Thira Jearsiripongkul [C]

[a] Department of Civil Engineering, Thammasat School of Engineering, Faculty of Engineering, Thammasat University, Pathumthani 12121, Thailand.

[b] Department of Engineering, School of Physics, Engineering and Computer Science, University of Hertfordshire, Hatfield AL10 9AB, England, United Kingdom.

[C] Department of Mechanical Engineering, Thammasat School of Engineering, Faculty of Engineering, Thammasat University, Pathumthani 12121, Thailand.

*Corresponding authors: P. R. Saffari, E-mail: rpeyman@engr.tu.ac.th

S.O. Ismail, E-mail: s.ismail3@herts.ac.uk

C. Thongchom, E-mail: Tchanach@engr.tu.ac.th

Abstract

In this study, the free vibration of a functionally graded carbon nanotube-reinforced composite (FG-CNTRC) sandwich nanoplate with an electrorheological fluid (ERF) layer as its core under a longitudinal magnetic field is examined using the nonlocal elasticity theory, Hamilton's principle, the third-order shear deformation theory (TSDT), and for various boundary conditions. While the continuity of physical quantities is required between all layers, the rule of mixing allows us to analyze the distribution of characteristics in this system's thickness direction. Changing the electric field also alters the ERF parameters in the pre-yield region. The generated equations are then solved using the Galerkin technique. A comparison with some other item of existing literature is used to evaluate the established solution's accuracy and correctness. The dependency of vibration behavior on certain factors: electric field strength, boundary conditions, magnetic field intensity, volume fraction of the carbon nanotubes (CNTs), CNTs distribution and nonlocal parameter are analyzed in a comprehensive parametric study.

Keywords: Electrorheological fluid; FG-CNTRC nanoplate; Free vibration; Nonlocal elasticity theory; Third-order shear deformation theory.

1. Introduction

Designing lightweight structures has been a critical area of concern for engineers for a long time. For example, reducing the weights of an airplane and a submarine directly supports the decrease in their fuel consumption. However, as these structures are generally built for a few load cases, they are prone to all kinds of vibrations. Apart from the passive control, which relies on altering material characteristics, especially damping and stiffness, active control has become an increasingly interesting topic ever since smart materials were introduced [1–3]. The former type of control is usually unable to tackle severe changes in loads, whereas the latter allows the implementation of different smart materials, such as electrorheological fluids (ERFs) or piezoelectric materials in most existing systems in order to adapt to any significant change in their surroundings. ERFs are smart materials of immense potential, especially in engineering fields. ERFs are made up of particles that may be electrically polarized and that are suspended in an insulating liquid. Atomic processes and ionic or electronic conduction are the sources of particle polarization in ERFs. In the absence of an electric field, they show low viscosity, while a specific electric field increases their viscosity by changing the state of particles [4–6]. Most ERFs used presently are made up of solids suspended in a liquid, so they need to be stabilized to keep them from settling. When an electric field of certain magnitude influences these two phases, it is expected to observe a material resembling a gel [7–9]. Yeh and Chen [10] examined how the electric field affected the natural frequency of a sandwich ERF plate and found that the natural frequency rises by increasing the electric field. The nonlinear dynamic response of a rotating sandwich beam with an ERF core was demonstrated by Wei et al. [11] using the finite element method (FEM). To study the damping and dynamic characteristics of the orthotropic cylindrical sandwich shells with an ERF core layer, Yeh [12] employed the classical thin shell theory. To analyze the fundamental frequencies of an ERF plate integrated with CNT-reinforced nanocomposite layers, Arani et al. [13] presented a numerical model using Eshelby-Mori-Tanaka technique and classical plate model. Forced and free vibration issues of a ERF plate with functionally graded (FG) face layers under a simply supported boundary condition were investigated by Babaki and Shakouri [14]. Based on the first-order shear deformation theory (FSDT), Shahali et al. [15] proposed a semi-analytical approach for analyzing the influences of the gradient factor and applied electric field on the variations of the modal loss factors and natural frequencies of a ERF cylinder with FG face layers. Khorshidi et al. [16] investigated the nonlinear vibration analysis of a sandwich ERF plate in contact with quiescent fluid using nonlinear Von-Karman strains and higher-order shear deformable theory. Ghavidel et al. [17] applied FSDT to study free vibration and damping behavior of cylindrical sandwich panel with ERF core and graphene platelets reinforced composite facing sheets.

Carbon nanotubes (CNTs) are small cylinder-shaped structures made up of rolled-up sheets of single-layer carbon atoms. Their notable properties are strong durability and aspect ratio, stiffness, and minimal density [18–21]. Chang et al. [22] provided closed-form formulas for the elastic characteristics of chiral SNTs. The aforementioned expressions exhibit concision while effectively establishing a direct correlation between material properties across varying length scales. Ghavanloo and Fazelzadeh [23] proposed an anisotropic elastic shell model utilizing the Flügge shell concept and complex method to investigate the vibration characteristics of chiral Single-wall carbon nanotubes (SWCNTs). In the study conducted by Strozzi et al. [24], a novel nonlocal anisotropic elastic shell model was formulated to analyze the nonlinear vibrations of double-walled carbon nanotubes (DWCNTs) using the Sanders-Koiter shell theory framework. Within the past few decades, analysts have paid much consideration to the advancement of fiber-reinforced composites. Standard filaments are normally made from glass, alumina, boron and silicon carbide, among others, as fillers in such composites. These common place filaments are in mesoscale with different diameters and lengths [25–27]. At the visible level, because reinforcements are distributed uniformly or randomly throughout the system, traditional composites' mechanical, physical, and thermal characteristics do not vary considerably. In order to ameliorate this characteristic, functionally graded materials (FGMs) have been developed [28–32]. They are made of two or more constituents with properties that can change spatially, which can be a non-uniform distribution of reinforcements. This technique allows engineers to obtain materials that act better than their homogenous counterparts. FG-carbon nanotube reinforced composite (FG-CNTRC) is a new class of high-stiffness materials that was created as a result of the combination of FGMs with carbon nanotubes [33–35]. The incorporation of CNTs in the composite material provides several advantages, such as enhanced mechanical properties, electrical conductivity, and thermal conductivity. Shen [33] presented the first study on FG-CNTRC and suggested a certain pattern of carbon nanotubes in an isotropic matrix based on equations that were already known to go in any direction. Mehar et al. [36] computed the fundamental frequencies of FG-CNTRC plate under thermal environment. Fu et al. [37] used FSDT and the generalized differential quadrature (GDQ) scheme for examining how FG-CNTRC annular sector plates buckle and vibrate. Based on the FSDT and irregular rational B-Spline foundational operations, Nguyen et al. [38] analyzed the natural frequencies and static performance of FG-CNTRC doubly-curved shell. The influences of the temperature, gradation function and inhomogeneity constraints on the static deflection and elastic instability of FG-CNTRC plates have been reported by Daikh et al. [39] utilizing Galerkin method. Huan et al. [40] used four-variable shear deformation refined model to solve the problem of FG-CNTRC plates vibrating in a fluid medium.

Besides, the manipulation of matter on small scales, also known as nanotechnology, has allowed to produce an extensive array of engineered materials, structures, devices and complicated systems that were otherwise impossible to realize [41,42]. On this small scale, experimental studies require a considerable amount of time, effort and money, especially when dealing with a large-scale molecular simulation. Furthermore, it has been shown that if the theories of classical continuum mechanics are employed, accurate prediction of material behavior on such scales is impossible. Therefore, researchers have considered non-classical

continuum theories that can effectively incorporate the interaction between atoms and molecules. Some of these non-classical continuum models are strain gradient theory (SGT) [43,44], Eringen's nonlocal elasticity model [45–47], modified strain gradient theory (MSGT) [48–52], modified couple stress theory (MCST) [53,54] and nonlocal strain gradient theory (NSGT) [55–58]. In accordance with Eringen's nonlocal theorem, a nonlocal parameter associated with the stiffness-softening effects is required to account for small-scale effects. The stress at one place in the continuum is a result of the strain at all other sites due to atomic forces and other small-scale variables, as the theory's fundamental notion makes clear. In line with third-order shear deformation theory (TSDT) and nonlocal elasticity theory, Aghababaei and Reddy [59] calculated the natural frequencies of a plate. FG-CNTRC nanoplates can be used in the construction of lightweight, high-strength materials for aerospace and defense applications. Phung-Van et al. [60] carried out the influence of the nonlocal term on the natural frequencies of an FG-CNTRC nanoplate applying nonlocal elasticity theory. Phung-Van et al. [61] investigated the dynamic behavior of an FG-CNTRC nanoplate under a homogeneous transverse force, considering temperature environment, nonlocal model of Eringen. Thai et al. [62] suggested meshfree approach with size dependence to investigate the bending behavior and natural frequencies of FG-CNTRC nanoplates.

The aforementioned literature established that although there exists an extensive body of researches on free vibration of sandwich ERF plates, but the free vibration of a FG-CNTRC sandwich nanoplate with an ERF core layer based on the TSDT and nonlocal elasticity model and undergoing a longitudinal magnetic field has not been investigated, using theoretical or numerical methods. To fill this knowledge gap, the current work proposes a unique combination of existing methods. The ERF properties in the pre-yield region change by varying the electric field and four different kinds of CNTs distributions are applied. A set of systematic analyses of the impacts of the boundary conditions, magnetic field intensity, CNTs distribution, electric field strength and nonlocal term on the natural frequency are also investigated.

The paper is structured as follows: In section 2, the methodology and main formulations of a FG-CNTRC sandwich nanoplate with an ERF core layer are presented. Then, the solution of the free vibration problem for different boundary conditions is provided in section 3. Section 4 presents a thorough comparative analysis and related parametric findings. Finally, conclusions are expressed in section 5.

2. Problem description and modeling

Fig. 1 depicts the dimensions and geometry of a sandwich rectangular nanoplate ($L_x \times L_y$) made up of three layers: a base FG-CNTRC layer (h_3), an ERF core layer (h_2), and a constraining FG-CNTRC layer (h_1). UD-CNTRC, as shown in Fig. 1, refers to a distribution scheme in which CNTs are uniformly distributed across the composite layer, whereas FG-V-CNTRC, FGX-CNTRC, and FG-O-CNTRC all include distributions of CNTs. No sliding is assumed to occur between the FG-CNTRC and ERF layers. As a result, all points on the cross section of all layers have the same transverse displacement.

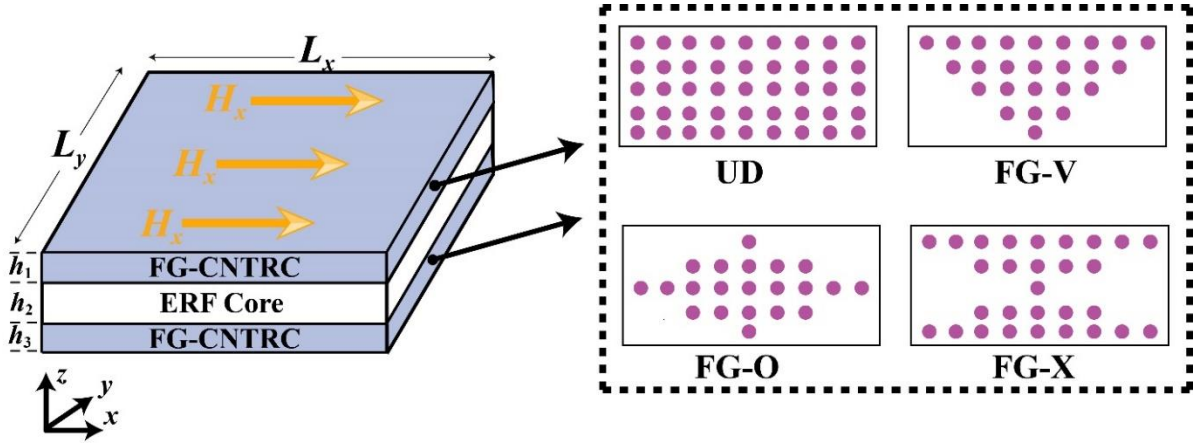

Fig. 1. Configuration of an FG-CNTRC sandwich nanoplate with ERF core layer.

2.1. Structural model

The rotating inertia and transverse shear deformation are both considered by TSDT. However, based on TSDT, the total displacement components (U, V, W) in Cartesian coordinates can be expressed as [63]

$$\begin{aligned} U_i(x,y,z,t) &= u_{0i}(x,y,t) + z\theta_{xi}(x,y,t) - C_1 z^3\left(\theta_{xi}(x,y,t) + \frac{\partial W_{0i}(x,y,t)}{\partial x}\right), \\ V_i(x,y,z,t) &= v_{0i}(x,y,t) + z\theta_{yi}(x,y,t) - C_1 z^3\left(\theta_{yi}(x,y,t) + \frac{\partial W_{0i}(x,y,t)}{\partial y}\right), \\ W_i(x,y,z,t) &= W_0(x,y,t), \quad i = b,c,t. \end{aligned} \tag{1}$$

where u_0 and v_0 are, respectively, the membrane deflections around the x-axis and y-axis. Furthermore, $C_1 = \frac{4}{3{h_j}^2}, (j = 1,2,3)$ and b, c and t denote, respectively, the bottom, core and top layers. The transverse displacement factor is denoted by W_0, whereas rotations of the central plane about the y- and x-axes are denoted by θ_y and θ_x. As previously stated, it is supposed that there is no slipping between the FG-CNTRC and ERF layers, consequently, through the thickness, the deformation distribution is continuous. Accordingly, displacement continuity condition in the FG-CNTRC/ERF interfaces can be resulted as

$$\begin{aligned} u_{0c} - \frac{h_2}{2}\theta_{xc} - \frac{h_2}{6}\left(\theta_{xc} + \frac{\partial W_0}{\partial x}\right) &= u_{0b} + \frac{h_3}{2}\theta_{xb} + \frac{h_3}{6}\left(\theta_{xb} + \frac{\partial W_0}{\partial x}\right), \\ v_{0c} - \frac{h_2}{2}\theta_{yc} - \frac{h_2}{6}\left(\theta_{yc} + \frac{\partial W_0}{\partial y}\right) &= v_{0b} + \frac{h_3}{2}\theta_{yb} + \frac{h_3}{6}\left(\theta_{yb} + \frac{\partial W_0}{\partial y}\right), \\ u_{0c} + \frac{h_2}{2}\theta_{xc} + \frac{h_2}{6}\left(\theta_{xc} + \frac{\partial W_0}{\partial x}\right) &= u_{0t} - \frac{h_1}{2}\theta_{xt} + \frac{h_1}{6}\left(\theta_{xt} + \frac{\partial W_0}{\partial x}\right), \\ v_{0c} + \frac{h_2}{2}\theta_{yc} + \frac{h_2}{6}\left(\theta_{yc} + \frac{\partial W_0}{\partial y}\right) &= v_{0t} - \frac{h_1}{2}\theta_{yt} + \frac{h_1}{6}\left(\theta_{yt} + \frac{\partial W_0}{\partial y}\right), \end{aligned} \tag{2}$$

which results in

$$\begin{aligned} u_{0c} &= \frac{1}{4}(u_{0t} + 3u_{0b}) - \frac{h_1}{3}\theta_{xt} + \frac{h_3}{3}\theta_{xb} - \frac{1}{12}\frac{\partial W_0}{\partial x}(h_1 - h_3), \\ v_{0c} &= \frac{1}{4}(v_{0t} + 3v_{0b}) - \frac{h_1}{3}\theta_{yt} + \frac{h_3}{3}\theta_{yb} - \frac{1}{12}\frac{\partial W_0}{\partial y}(h_1 - h_3), \end{aligned}$$

$$\theta_{xc} = \frac{3}{4h_2}(u_{0t} - u_{0b}) - \frac{1}{2h_2}(h_1\theta_{xt} + h_3\theta_{xb}) - \frac{1}{4}\frac{\partial W_0}{\partial x}\left(1 + \frac{h_1}{2h_2} + \frac{h_3}{2h_2}\right), \tag{3}$$

$$\theta_{yc} = \frac{3}{4h_2}(v_{0t} - v_{0b}) - \frac{1}{2h_2}\left(h_1\theta_{yt} + h_3\theta_{yb}\right) - \frac{1}{4}\frac{\partial W_0}{\partial y}\left(1 + \frac{h_1}{2h_2} + \frac{h_3}{2h_2}\right),$$

The following is a definition of the strain elements in FG-CNTRC layers:

$$\varepsilon_{xxi} = \frac{\partial u_{0i}}{\partial x} + z\frac{\partial \theta_{xi}}{\partial x} - C_1 z^3\left(\frac{\partial \theta_{xi}}{\partial x} + \frac{\partial^2 W_0}{\partial x^2}\right),$$

$$\varepsilon_{yyi} = \frac{\partial v_{0i}}{\partial y} + z\frac{\partial \theta_{yi}}{\partial y} - C_1 z^3\left(\frac{\partial \theta_{yi}}{\partial y} + \frac{\partial^2 W_0}{\partial y^2}\right),$$

$$\gamma_{xyi} = \frac{\partial u_{0i}}{\partial y} + \frac{\partial v_{0i}}{\partial x} + z\left(\frac{\partial \theta_{xi}}{\partial y} + \frac{\partial \theta_{yi}}{\partial x}\right) - C_1 z^3\left(\frac{\partial \theta_{xi}}{\partial y} + \frac{\partial \theta_{yi}}{\partial x} + 2\frac{\partial^2 W_0}{\partial x \partial y}\right), \tag{4}$$

$$\gamma_{xzi} = (1 - 3C_1 z^2)\left(\theta_{xi} + \frac{\partial W_0}{\partial x}\right),$$

$$\gamma_{yzi} = (1 - 3C_1 z^2)\left(\theta_{yi} + \frac{\partial W_0}{\partial y}\right). \quad i = b, t.$$

As well, for the ERF layer, the transverse shear strain elements may be written as

$$\gamma_{xzc} = (1 - 3C_1 z^2)\left(\theta_{xc} + \frac{\partial W_0}{\partial x}\right) = (1 - 3C_1 z^2)\left[\frac{3}{4h_2}(u_{0t} - u_{0b}) - \frac{1}{2h_2}(h_1\theta_{xt} + h_3\theta_{xb}) - \frac{1}{4}\frac{\partial W_0}{\partial x}\left(-3 + \frac{h_1}{2h_2} + \frac{h_3}{2h_2}\right)\right],$$

$$\gamma_{yzc} = (1 - 3C_1 z^2)\left(\theta_{yc} + \frac{\partial W_0}{\partial y}\right) = (1 - 3C_1 z^2)\left[\frac{3}{4h_2}(v_{0t} - v_{0b}) - \frac{1}{2h_2}\left(h_1\theta_{yt} + h_3\theta_{yb}\right) - \frac{1}{4}\frac{\partial W_0}{\partial y}\left(-3 + \frac{h_1}{2h_2} + \frac{h_3}{2h_2}\right)\right]. \tag{5}$$

The nonclassical basic stress-strain relationships containing normal $(\sigma_{xx}, \sigma_{\theta\theta})$ and shear $(\tau_{xz}, \tau_{\theta z}, \tau_{x\theta})$ stress components for each FG-CNTRC layer in accordance with the nonlocal elasticity model of Eringen, are given as [64]

$$[1 - (e_0 a)^2\nabla^2]\begin{bmatrix}\sigma_{xxi}\\ \sigma_{yyi}\\ \tau_{xyi}\\ \tau_{yzi}\\ \tau_{xzi}\end{bmatrix} = \begin{Bmatrix}Q_{11} & Q_{12} & 0 & 0 & 0\\ Q_{21} & Q_{22} & 0 & 0 & 0\\ 0 & 0 & Q_{66} & 0 & 0\\ 0 & 0 & 0 & Q_{44} & 0\\ 0 & 0 & 0 & 0 & Q_{55}\end{Bmatrix}\begin{bmatrix}\varepsilon_{xxi}\\ \varepsilon_{yyi}\\ \gamma_{xyi}\\ \gamma_{yzi}\\ \gamma_{xzi}\end{bmatrix}, \ i = b, t. \tag{6}$$

$$Q_{11} = \frac{E_{11}}{1 - \vartheta_{12}\vartheta_{21}}, Q_{22} = \frac{E_{22}}{1 - \vartheta_{12}\vartheta_{21}}, Q_{12} = \frac{\vartheta_{12}E_{22}}{1 - \vartheta_{12}\vartheta_{21}}, Q_{66} = G_{12}, Q_{44} = G_{23}, Q_{55} = G_{13}$$

Here, $e_0 a$ and e_0 are, respectively, the nonlocal parameter and the calibration constant. These parameters can be changed to verify other reported models in the literature. For instance, Eringen [45,46] has mentioned a value of 0.39 for e_0. Moreover, a is the internal effective length. If a is much smaller than its external counterpart, the traditional elasticity and nonlocal models become identical. If the external and internal effective lengths are relatively close, the nonlocal elasticity theory matches the theory of lattice dynamics [65,66]. The inclusion of Lamé parameters and one or more length scale parameters allow us to study the nano scale effects in a nonlocal elasticity theory. At this point, the effective Young's modulus of the FG-CNTRC layer is denoted by E_{11} and E_{22}; Poisson's ratio is indicated by ϑ_{12} and ϑ_{21}; and the shear modulus is shown by G_{12}, G_{23}, and G_{13}. Applying the rule of mixture, such material characteristics of FG-CNTRC layer are defined as [67]

$$E_{11} = \zeta_1 V_{CNT} E_{11}^{CNT} + V_m E_m,$$

$$\frac{\zeta_2}{E_{22}} = \frac{V_{CNT}}{E_{22}^{CNT}} + \frac{V_m}{E_m},$$
$$\frac{\zeta_3}{G_{12}} = \frac{V_{CNT}}{G_{12}^{CNT}} + \frac{V_m}{G_m}, \tag{7}$$

where the material properties of CNTs are denoted with $(E_{11}^{CNT}, E_{22}^{CNT}, G_{12}^{CNT})$, and the isotropic matrix moduli are expressed by (E_m, G_m). Furthermore, the parameters for CNT efficiency are ζ_1, ζ_2, and ζ_3, and

$$V_m + V_{CNT} = 1, \tag{8}$$
$$\vartheta_{12} = V_{CNT}^{*}\vartheta_{12}^{CNT} + V_m\vartheta_m,$$

where V_{CNT}^{*} and V_{CNT} represent the volume fractions of the FG-O, FG-X, UD, and FG-V patterns of the FG-CNTRC [67]

$$V_{CNT} = \begin{cases} V_{CNT}^{*} & (\mathrm{UD}) \\ \left(1 + \frac{2z}{h_c}\right) V_{CNT}^{*}, & (\mathrm{FG-V}) \\ 2\left(1 - \frac{2|z|}{h_c}\right) V_{CNT}^{*}, & (\mathrm{FG-O}) \\ 4\frac{|z|}{h_c} V_{CNT}^{*}, & (\mathrm{FG-X}) \end{cases} \tag{9}$$

Comparatively, in the ERF layer, the nonclassical transverse shear stresses are given as [10,68]

$$[1 - (e_0 a)^2\nabla^2]\tau_{xzc} = G^{(c)}\gamma_{xzc}, \;\; [1 - (e_0 a)^2\nabla^2]\tau_{yzc} = G^{(c)}\gamma_{yzc} \tag{10}$$

in which $G^{(c)}$ refers to the complex shear modulus of the electric field-dependent ERF. Using Maxwell's equations, we can calculate the Lorentz force that is generated when a longitudinal magnetic field with intensity of $(H_x, 0,0)$ is applied to the sandwich plate [69]. Additionally, it is supposed that the Lorentz force only acts in the z direction on the structure as

$$f_z = \eta H_x^2\left(\frac{\partial^2 W_i}{\partial x^2} + \frac{\partial^2 W_i}{\partial z^2} + \frac{\partial^2 V_i}{\partial z \partial y}\right) = \eta H_x^2\left(\frac{\partial^2 W_0}{\partial x^2} + \frac{\partial \theta_{yi}}{\partial y} - 2C_1 z^2\frac{\partial \theta_{yi}}{\partial y}\right), \;\; i = b, c, t. \tag{11}$$

where the magnetic field permeability is expressed by η. The final form of the equilibrium equations for the studied structure is obtained in this section by using the Hamilton's principle [70,71].

$$\int_{t_0}^{t}(\delta\Pi_T - \delta\Pi_V + \delta\Pi_F)dt = 0. \tag{12}$$

where Π_V signifies the virtual strain energy, Π_T expresses the virtual kinetic energy; Π_F displays the virtual work applied by mechanical loads. The kinetic energy for ERF sandwich nanoplate can be presented as

$$\Pi_T = \frac{1}{2}\int_{A_b}\int_{-h_3/2}^{h_3/2}\rho\left(\dot{U}_b{}^2 + \dot{V}_b{}^2 + \dot{W}_b{}^2\right)dzdA_b + \frac{1}{2}\int_{A_c}\int_{-h_2/2}^{h_2/2}\rho_f\dot{W}_c{}^2\,dzdA_c + \frac{1}{2}\int_{A_t}\int_{-h_1/2}^{h_1/2}\rho\left(\dot{U}_t{}^2 + \dot{V}_t{}^2 + \dot{W}_t{}^2\right)dzdA_t, \tag{13}$$

However, the variation of kinetic energy for ERF sandwich nanoplate is expressed as

$$\delta\Pi_T = \int_{A_b}\int_{-h_3/2}^{h_3/2}\rho\left[\dot{U}_b\delta\dot{U}_b + \dot{V}_b\delta\dot{V}_b + \dot{W}_b\delta\dot{W}_b\right]dz\mathrm{d}A_b + \int_{A_c}\int_{-h_2/2}^{h_2/2}\rho_f\,\dot{W}_c\delta\dot{W}_c dz\mathrm{d}A_c + \int_{A_t}\int_{-h_1/2}^{h_1/2}\rho\left[\dot{U}_t\delta\dot{U}_t + \dot{V}_t\delta\dot{V}_t + \dot{W}_t\delta\dot{W}_t\right]dz\mathrm{d}A_t, \quad (14)$$

where ρ_f signifies the mass density of ERF layer, cross-sectional area is represented by A, and ρ indicates the FG-CNTRC layer's mass density, which is presented as

$$\rho = V_{CNT}\rho^{CNT} + V_m\rho_m. \quad (15)$$

The strain energy can be calculated by integrating the stress-strain curve of the material over the region of elastic deformation as follows

$$\Pi_V = \int_{A_b}\int_{-h_3/2}^{h_3/2}\left(\sigma_{xxb}\varepsilon_{xxb} + \sigma_{yyb}\varepsilon_{yyb} + \tau_{yzb}\gamma_{yzb} + \tau_{xzb}\gamma_{xzb} + \tau_{xyb}\gamma_{xyb}\right)dz\mathrm{d}A_b + \int_{A_c}\int_{-h_2/2}^{h_2/2}\left(\tau_{yzc}\gamma_{yzc} + \tau_{xzc}\gamma_{xzc}\right)dz\mathrm{d}A_c + \int_{A_t}\int_{-h_1/2}^{h_1/2}\left(\sigma_{xxt}\varepsilon_{xxt} + \sigma_{yyt}\delta\varepsilon_{yyt} + \tau_{yzt}\gamma_{yzt} + \tau_{xzt}\gamma_{xzt} + \tau_{xyt}\gamma_{xyt}\right)dz\mathrm{d}A_t, \quad (16)$$

The entire strain energy's variation is written as

$$\delta\Pi_V = \int_{A_b}\int_{-h_3/2}^{h_3/2}\left(\sigma_{xxb}\delta\varepsilon_{xxb} + \sigma_{yyb}\delta\varepsilon_{yyb} + \tau_{yzb}\delta\gamma_{yzb} + \tau_{xzb}\delta\gamma_{xzb} + \tau_{xyb}\delta\gamma_{xyb}\right)dz\mathrm{d}A_b + \int_{A_c}\int_{-h_2/2}^{h_2/2}\left(\tau_{yzc}\delta\gamma_{yzc} + \tau_{xzc}\delta\gamma_{xzc}\right)dz\mathrm{d}A_c + \int_{A_t}\int_{-h_1/2}^{h_1/2}\left(\sigma_{xxt}\delta\varepsilon_{xxt} + \sigma_{yyt}\delta\varepsilon_{yyt} + \tau_{yzt}\delta\gamma_{yzt} + \tau_{xzt}\delta\gamma_{xzt} + \tau_{xyt}\delta\gamma_{xyt}\right)dz\mathrm{d}A_t, \quad (17)$$

Lastly, the variation of virtual work, due to mechanical loads, is stated as

$$\delta\Pi_F = \int_A q\delta W_0\mathrm{d}A, \quad (18)$$

where $q = \int_{-h_3/2}^{h_1/2} f_z dz$. However, substituting Eqs (14), (17) and (18) into Eq. (12), performing some manipulations, and by taking into account the coefficients $\delta u_{0b}, \delta u_{0t}, \delta v_{0b}, \delta v_{0t}, \delta W_0, \delta\theta_{xb}, \delta\theta_{xt}, \delta\theta_{yb}$ and $\delta\theta_{yt}$ equal to zero, the governing equations are ultimately obtained and provided in Appendix A. Lastly, replacing Eq. (A10) into Eqs. (A1-A9), and considering Eqs (1-6), assuming $h_3 = h_1$, the size-dependent equations for sandwich nanoplate are attained and expressed in Appendix B.

3. Solution method

The process of solving the derived equations requires proper definitions of boundary conditions. Therefore:

Clamped (C) edge boundary conditions

$$u_{0t} = u_{0b} = v_{0t} = v_{0b} = W_0 = \theta_{xt} = \theta_{xb} = \theta_{yt} = \theta_{yb} = 0, \quad at\ x = 0, L_x;\ \ y = 0, L_y. \quad (19)$$

Simply supported (S) edge boundary conditions

$$v_{0t} = v_{0b} = W_0 = \theta_{yt} = \theta_{yb} = N_{xxt} = N_{xxb} = M_{xxt} = M_{xxb} = P_{xxt} = P_{xxb} = 0, \quad at\ x = 0, L_x,$$
$$u_{0t} = u_{0b} = W_0 = \theta_{xt} = \theta_{xb} = N_{yyt} = N_{yyb} = M_{yyt} = M_{yyb} = P_{yyt} = P_{yyb} = 0, \quad at\ y = 0, L_y. \quad (20)$$

For the relevant boundary conditions, the following suitable formulations are used [72,73]

$$u_{0t} = \sum_m^\infty \sum_n^\infty \widetilde{U}_t \frac{\partial X_m(x)}{\partial x} Y_n(y) e^{i\omega t}, \quad u_{0b} = \sum_m^\infty \sum_n^\infty \widetilde{U}_b \frac{\partial X_m(x)}{\partial x} Y_n(y) e^{i\omega t},$$

$$v_{0t} = \sum_m^\infty \sum_n^\infty \widetilde{V}_t X_m(x) \frac{\partial Y_n(y)}{\partial y} e^{i\omega t}, \quad v_{0b} = \sum_m^\infty \sum_n^\infty \widetilde{V}_b X_m(x) \frac{\partial Y_n(y)}{\partial y} e^{i\omega t},$$

$$W_0 = \sum_m^\infty \sum_n^\infty \widetilde{W} Y_n(y) X_m(x) e^{i\omega t}, \quad \theta_{xt} = \sum_m^\infty \sum_n^\infty \tilde{\theta}_{xt} \frac{\partial X_m(x)}{\partial x} Y_n(y) e^{i\omega t},$$

$$\theta_{xb} = \sum_m^\infty \sum_n^\infty \tilde{\theta}_{xb} \frac{\partial X_m(x)}{\partial x} Y_n(y) e^{i\omega t}, \quad \theta_{yt} = \sum_m^\infty \sum_n^\infty \tilde{\theta}_{yt} X_m(x) \frac{\partial Y_n(y)}{\partial y} e^{i\omega t}, \tag{21}$$

$$\theta_{yb} = \sum_m^\infty \sum_n^\infty \tilde{\theta}_{yb} X_m(x) \frac{\partial Y_n(y)}{\partial y} e^{i\omega t},$$

where the angular frequency is represented by ω. Correspondingly, the half wave numbers of x and y direction are, respectively, expressed by m and n. The set of variables $\left(\widetilde{U}_t, \widetilde{U}_b, \widetilde{V}_t, \widetilde{V}_b, \widetilde{W}, \tilde{\theta}_{xt}, \tilde{\theta}_{xb}, \tilde{\theta}_{yt} \text{ and } \tilde{\theta}_{yb}\right)$ are unknown modal coefficients for the considered sandwich nanoplate. X_m and Y_n are expressed as functions to satisfy the boundary conditions [72]

SSSS:

$$X_m(x) = sin\left(\frac{m\pi x}{L_x}\right), \; Y_n(y) = sin\left(\frac{n\pi y}{L_y}\right), \tag{22}$$

SSCS:

$$X_m(x) = sin\left(\frac{m\pi x}{L_x}\right), \quad Y_n(y) = \left[sin\left(\frac{(n+0.25)\pi y}{L_y}\right) - sinh\left(\frac{(n+0.25)\pi y}{L_y}\right)\right] - \left[\frac{sin((n+0.25)\pi)+sinh((n+0.25)\pi)}{cos((n+0.25)\pi)+cosh((n+0.25)\pi)}\right]\left[cos\left(\frac{(n+0.25)\pi y}{L_y}\right) - cosh\left(\frac{(n+0.25)\pi y}{L_y}\right)\right], \tag{23}$$

SSCC:

$$X_m(x) = sin\left(\frac{m\pi x}{L_x}\right), \; Y_n(y) = \left[sin\left(\frac{(n+0.5)\pi y}{L_y}\right) - sinh\left(\frac{(n+0.5)\pi y}{L_y}\right)\right] - \left[\frac{sin((n+0.5)\pi)-sinh((n+0.5)\pi)}{cos((n+025)\pi)-cosh((n+0.5)\pi)}\right]\left[cos\left(\frac{(n+0.5)\pi y}{L_y}\right) - cosh\left(\frac{(n+0.5)\pi y}{L_y}\right)\right], \tag{24}$$

CSCC:

$$X_m(x) = \left[sin\left(\frac{(n+0.25)\pi x}{L_x}\right) - sinh\left(\frac{(n+0.25)\pi x}{L_x}\right)\right] - \left[\frac{sin((n+0.25)\pi)+sinh((n+0.25)\pi)}{cos((n+0.25)\pi)+cosh((n+0.25)\pi)}\right]\left[cos\left(\frac{(n+0.25)\pi x}{L_x}\right) - cosh\left(\frac{(n+0.25)\pi x}{L_x}\right)\right], \tag{25}$$

$$Y_n(y) = \left[sin\left(\frac{(n+0.5)\pi y}{L_y}\right) - sinh\left(\frac{(n+0.5)\pi y}{L_y}\right)\right] - \left[\frac{sin((n+0.5)\pi)-sinh((n+0.5)\pi)}{cos((n+025)\pi)-cosh((n+0.5)\pi)}\right]\left[cos\left(\frac{(n+0.5)\pi y}{L_y}\right) - cosh\left(\frac{(n+0.5)\pi y}{L_y}\right)\right],$$

CCCC:

$$X_m(x) = \left[sin\left(\frac{(n+0.5)\pi x}{L_x}\right) - sinh\left(\frac{(n+0.5)\pi x}{L_x}\right)\right] - \left[\frac{sin((n+0.5)\pi) - sinh((n+0.5)\pi)}{cos((n+0.5)\pi) - cosh((n+0.5)\pi)}\right]\left[cos\left(\frac{(n+0.5)\pi x}{L_x}\right) - cosh\left(\frac{(n+0.5)\pi x}{L_x}\right)\right], \quad (26)$$

$$Y_n(y) = \left[sin\left(\frac{(n+0.5)\pi y}{L_y}\right) - sinh\left(\frac{(n+0.5)\pi y}{L_y}\right)\right] - \left[\frac{sin((n+0.5)\pi) - sinh((n+0.5)\pi)}{cos((n+025)\pi) - cosh((n+0.5)\pi)}\right]\left[cos\left(\frac{(n+0.5)\pi y}{L_y}\right) - cosh\left(\frac{(n+0.5)\pi y}{L_y}\right)\right],$$

The matrix representation of the equilibrium equations is found by substituting Eq. (21) in Eqs. (B1-B9). The final results are written as

$$([\mathbf{M}]_{9\times9}\omega^2 - [\mathbf{K}]_{9\times9})\bar{\mathbf{q}} = 0 \quad (27)$$

where the matrices $[\mathbf{K}]_{9\times9}$ and $[\mathbf{M}]_{9\times9}$ indicates, respectively, stiffness and mass and matrices. The natural frequencies, $\omega^* = \sqrt{\mathrm{Re}(\omega^2)}$ and the modal loss factors, $\eta_v = \frac{\mathrm{Im}(\omega^2)}{\mathrm{Re}(\omega^2)}$ are obtained from the non-trivial solution of Eq. (27). To achieve this aim, in the last equation, the left-side matrix's determinant should be set to zero, yielding the eigenfrequencies and eigenvectors.

4. Findings and discussion

This section is followed by a series of numerical investigations, according to the properties shown in Table 1 [74]. Furthermore, Table 2 denotes the characteristics of CNT efficiency for various volume fractions [67]. Moreover, Poly {(m-phenylenevinylene) -co- [(2.5-dioctoxy-p-phenylene) vinylene]} is considered as polymeric matrix [67].

Table 1: Material characteristics of an FG-CNTRC nanoplate with ERF core layer.

Properties (**ERF core Layer**)		
Shear modulus	$G^{(c)} = G'(\Xi) + iG''(\Xi)$, $G'(\Xi) = 50000\Xi^2$, $G''(\Xi) = 2600\Xi + 1700$	
Mass density (kg m^{-3})	$\rho_f = 1700$	
Properties (**FG-CNTRC**)	CNT	Poly Matrix
Elastic	$E_{11}^{CNT} = 5.6466$TPa, $E_{22}^{CNT} = 7.08$TPa, $G_{12}^{CNT} = 1.944$TPa	$E_m = 2.1$GPa,
Poisson's Ratio	$\vartheta_{12}^{CNT} = 0.175$	$\vartheta_m = 0.34$
Mass density (Kg m^{-3})	$\rho^{CNT} = 1400$	$\rho_m = 1160$

Table 2: Efficiency coefficients for different CNTs volume fractions.

V_{CNT}^*	Efficiency parameters		
	ζ_1	ζ_1	ζ_1
0.11	0.149	0.934	0.934
0.14	0.15	0.941	0.941
0.17	0.14	1.381	1.381

4.1 Validation of the model

The formulation validation is provided via the means of a few examples. As the first comparison study, by eliminating ERF and FG-CNTRC properties, the first three non-dimensional frequencies, $\bar{\omega} = \omega^* h_1 \sqrt{\rho / G_{12}}$ of an elastic nanoplate ($\frac{L_x}{L_y} = 1, L_x = 10h$) for various boundary conditions and nonlocal parameters are computed after which they were compared to those found in Ref. [72] as provided in Table 3. By comparing the current findings to the analytic predictions of Ref. [72], as shown in Table 3, we find that the current findings are quite close to those expected.

Table 3: Comparison of dimensionless natural frequency of an elastic nanoplate for different boundary conditions and nonlocal parameters.

B.C	$(e_0 a)^2 (nm^2)$	Study	$\bar{\omega}_1$	$\bar{\omega}_2$	$\bar{\omega}_3$
SSSS	0	present	0.092	0.221	0.338
		Ref. [72]	0.093	0.222	0.341
	2	present	0.078	0.157	0.210
		Ref. [72]	0.079	0.157	0.212
	4	present	0.069	0.128	0.166
		Ref. [72]	0.070	0.129	0.167
CSCS	0	present	0.125	0.267	0.389
		Ref. [72]	0.126	0.268	0.392
	2	present	0.104	0.184	0.235
		Ref. [72]	0.104	0.185	0.237
	4	present	0.903	0.149	0.184
		Ref. [72]	0.908	0.150	0.186
CCCC	0	present	0.161	0.313	0.442
		Ref. [72]	0.162	0.315	0.445
	2	present	0.132	0.212	0.261
		Ref. [72]	0.132	0.213	0.263
	4	present	0.114	0.171	0.203
		Ref. [72]	0.115	0.171	0.204

Considering another comparison investigation, by ignoring FG-CNTRC layers and nonlocal parameter, the natural frequencies (Hz) and the corresponding modal loss factor of a simply supported ERF sandwich plate for different aspect ratios and ERF core thickness terms are evaluated. Results from the present system are shown in Table 4 and evaluated with those from Ref. [74] that employ classical plate theory. It is significantly evident from this table that the proposed model in the present work has high accuracy in calculating the frequencies of the ERF plate. Another point of interest is that as the electric field intensifies, the natural frequency rises. This is because there has been a rise in the ERF's electric modulus.

Table 4: Comparison of natural frequencies (Hz) and the corresponding modal loss factor of the simply supported ERF sandwich plate versus the electric field.

Mode	h_2/h_1	L_y/L_x	$\Xi = 0\text{kV/mm}$				$\Xi = 2\text{kV/mm}$			
			ω^*, (Hz)		η_υ		ω^*, (Hz)		η_υ	
			Ref. [74]	present	Ref. [74]	present	Ref. [74]	present	Ref. [74]	present
(1,1)	1	1	13.1925	13.1926	0.0172	0.0172	21.8035	21.8041	0.0187	0.0187
		2	32.9809	32.9812	0.0069	0.0069	43.7317	43.7322	0.0139	0.0139
	4	1	10.0639	10.0646	0.0269	0.0269	20.2119	20.2140	0.0249	0.0249
		2	25.159	25.1604	0.0107	0.0107	37.6844	37.6867	0.0188	0.0188

(1,2)	1	1	32.9809	32.9806	0.0069	0.0069	43.7317	43.7323	0.0139	0.0139
		2	52.7693	52.7683	0.0043	0.0043	64.3128	64.3128	0.0108	0.0108
	4	1	25.159	25.1600	0.0107	0.0107	37.6844	37.6875	0.0188	0.0188
		2	40.2533	40.2554	0.0067	0.0067	53.736	53.7402	0.015	0.015
(2,2)	1	1	52.7693	52.7694	0.0043	0.0043	64.3128	64.3133	0.0108	0.0108
		2	131.922	131.918	0.0017	0.0017	144.452	144.446	0.0056	0.0056
	4	1	40.2533	40.2563	0.0067	0.0067	53.736	53.7412	0.015	0.015
		2	100.623	100.636	0.0027	0.0027	115.379	115.396	0.0082	0.0082

Also, Table 5 presents the dimensionless frequencies, $\bar{\omega} = \omega^* \frac{{L_x}^2}{h_1} \sqrt{\rho_m / E_m}$ of an FG-CNTRC square plate at various boundary conditions for four categories of CNTRC when the properties of ERF core layer and nonlocal parameter are neglected. Comparison of the outcomes of the current formulation and those presented by Ref. [67] clearly support the acceptable performance of the developed formulation.

Table 5: Comparison of dimensionless natural frequency of an FG-CNTRC plate for four types of CNTRC.

B.C	V^*_{CNT}	h_1/L_x	UD		FG-V		FG-O		FG-X	
			Ref. [67]	present	Ref. [67]	present	Ref. [67]	present	Ref. [67]	present
SSSS	0.11	0.1	14.024	13.882	12.755	12.793	11.773	11.701	15.254	15.213
		0.05	17.503	17.711	15.127	15.291	13.500	13.625	20.241	20.342
	0.14	0.1	14.925	14.770	13.653	13.607	12.662	12.501	16.104	16.008
		0.05	19.196	19.248	16.606	16.724	14.838	14.933	22.084	22.192
	0.17	0.1	17.409	17.301	15.788	15.616	14.563	14.432	18.969	18.851
		0.05	21.624	21.738	18.632	18.675	16.625	16.705	25.049	24.966
CCCC	0.11	0.1	19.473	19.515	18.811	18.976	18.198	18.056	20.195	20.308
		0.05	30.391	30.405	27.709	27.816	25.592	25.634	32.901	33.005
	0.14	0.1	20.112	20.194	19.516	19.588	18.962	19.071	20.566	20.611
		0.05	32.268	32.299	29.627	29.722	27.517	27.546	34.639	34.702
	0.17	0.1	24.299	24.364	23.437	23.509	22.655	22.697	24.970	25.007
		0.05	37.741	37.831	34.300	34.386	31.644	31.681	40.936	41.064

4.2. Parametric study

To describe the structure's free vibration behavior in response to various factors, parametric analyses are carried out. Tables 6 and 7 present the corresponding modal loss factor and natural frequency of the system under different boundary conditions, thickness ratios, electric field strengths ($\Xi = 0,1.5,3,4.5$) and the CNTs distributions, when $h_1 = h_3 = 1$ nm, $L_x = L_y = 10$ nm, $H_x = 0, e_0 a = 0, V^*_{CNT} = 0.11$. Both geometric aspect ratio and electric field intensity are directly proportional to the natural frequency. By decreasing mode number, the effect of the electric field on the natural frequency becomes more pronounced. More also, the value of the geometric thickness ratio determines the impact of the electric field on the modal loss factor. It appears that the loss factor grows at small electric fields, then it peaks at a medium electric field, and finally decreases with at higher values of electric field intensity. The structural stiffness is strongly dependent upon the CNTs distribution. Natural frequencies' smallest and greatest ranges belong to FG-O and FG-X distributions, respectively. Actually, in FG-X case, each FG-CNTRC layer's top and bottom surfaces have the highest volume fractions, bringing about a larger structural stiffness and system strength. However, it can be observed that the

boundary conditions have important effects on the variations of the natural frequencies. It also seems that the loss factor behavior is opposite to the natural frequency under different boundary conditions and the CNTs distributions. The described concepts of this analytical study can also be used to better understand the vibration behavior. The thickness ratio ($\frac{h_2}{h_1}$) strongly affects the natural frequency. This article also provides valuable insight into the potential applications of CNTs, including the structural parts of different sensors and nanodevices.

Table 6: The effects of the electric field, thickness ratio, mode number, and CNTs distributions on the natural frequency and modal loss factor (SSSS).

Type	Mode	h_2/h_1	$\Xi = 0$		$\Xi = 1.5$		$\Xi = 3$		$\Xi = 4.5$	
			ω^*, (GHz)	η_υ	ω^*, (GHz)	η_υ	ω^*, (GHz)	η_υ	ω^*, (GHz)	η_υ
UD	(1,1)	1	23.747	0.011	24.563	0.023	26.503	0.029	28.794	0.031
		4	15.848	0.020	16.880	0.042	19.545	0.058	23.046	0.059
	(1,2)	1	30.878	0.0017	32.607	0.0036	36.913	0.0048	42.187	0.005
		4	20.668	0.0031	22.689	0.0061	27.777	0.0077	34.353	0.008
	(2,2)	1	61.346	0.0014	62.416	0.0024	65.308	0.0033	69.314	0.0038
		4	41.053	0.0021	42.552	0.0032	46.703	0.0040	52.738	0.0045
FG-V	(1,1)	1	21.746	0.0138	22.677	0.0277	24.880	0.0357	27.471	0.0372
		4	14.516	0.0242	15.657	0.0456	18.549	0.0595	22.278	0.0611
	(1,2)	1	29.620	0.0020	31.443	0.0041	35.953	0.0052	41.442	0.0055
		4	19.831	0.0034	21.940	0.0065	27.198	0.0079	33.924	0.0081
	(2,2)	1	59.535	0.0018	60.665	0.0027	63.723	0.0043	67.958	0.0047
		4	39.848	0.0026	41.408	0.0037	45.710	0.0046	51.929	0.0049
FG-O	(1,1)	1	20.160	0.017	21.194	0.0329	23.629	0.0413	26.471	0.0435
		4	13.457	0.029	14.695	0.057	17.784	0.061	21.697	0.0635
	(1,2)	1	28.274	0.0022	30.206	0.0043	34.947	0.0054	40.666	0.0056
		4	18.928	0.0038	21.142	0.0067	26.589	0.0082	33.477	0.0083
	(2,2)	1	57.596	0.0021	58.798	0.0029	62.044	0.0044	66.527	0.0048
		4	38.552	0.0031	40.180	0.0042	44.650	0.0049	51.068	0.0051
FG-X	(1,1)	1	25.674	0.0091	26.396	0.0185	28.117	0.024	30.152	0.025
		4	17.132	0.017	18.074	0.036	20.541	0.052	23.837	0.056
	(1,2)	1	32.512	0.0015	34.131	0.0033	38.196	0.0045	43.220	0.0048
		4	21.761	0.0028	23.675	0.0056	28.555	0.0071	34.494	0.0077
	(2,2)	1	63.157	0.0011	64.171	0.0021	66.918	0.0030	70.725	0.0035
		4	42.263	0.0017	43.705	0.0029	47.716	0.0037	53.581	0.0043

Table 7: The effects of the electric field, thickness ratio, mode number and CNTs distributions on the natural frequency and modal loss factor (CCCC).

Type	Mode	h_2/h_1	$\Xi = 0$		$\Xi = 1.5$		$\Xi = 3$		$\Xi = 4.5$	
			ω^*, (GHz)	η_υ	ω^*, (GHz)	η_υ	ω^*, (GHz)	η_υ	ω^*, (GHz)	η_υ
UD	(1,1)	1	33.787	0.0006	34.440	0.0125	36.052	0.0199	38.322	0.0224
		4	22.545	0.0012	23.397	0.0257	25.747	0.0407	29.146	0.0454
	(1,2)	1	43.036	0.0004	44.360	0.0105	47.911	0.0142	52.767	0.0198
		4	28.798	0.0008	30.464	0.0163	34.932	0.0257	41.162	0.0306
	(2,2)	1	71.679	0.0003	72.656	0.0088	75.387	0.0111	79.387	0.0163
		4	47.958	0.0004	49.410	0.0124	53.495	0.0187	59.584	0.0225
FG-V	(1,1)	1	32.670	0.0009	33.323	0.0156	35.080	0.0226	37.491	0.0249
		4	21.803	0.0015	22.692	0.0279	25.138	0.0420	28.652	0.0463
	(1,2)	1	42.319	0.0005	43.676	0.0121	47.313	0.0159	52.277	0.0215
		4	28.319	0.0009	30.019	0.0175	34.563	0.0268	40.876	0.0310
	(2,2)	1	70.675	0.0004	71.681	0.0101	74.496	0.0136	78.616	0.0179
		4	47.289	0.0005	48.771	0.0132	52.934	0.0197	59.123	0.0240

FG-O	(1,1)	1	31.511	0.0012	32.208	0.0173	34.078	0.0241	36.640	0.0258
		4	21.028	0.0016	21.961	0.0296	24.510	0.0450	28.143	0.0487
	(1,2)	1	41.164	0.0006	42.580	0.0145	46.359	0.0174	51.495	0.0229
		4	27.547	0.0012	29.303	0.0199	33.971	0.0295	40.414	0.0331
	(2,2)	1	69.272	0.0005	70.322	0.0251	73.256	0.0172	77.538	0.0196
		4	46.352	0.0006	47.877	0.0158	52.147	0.0213	58.470	0.0264
FG-X	(1,1)	1	34.853	0.0004	35.432	0.0108	36.994	0.0174	39.148	0.0209
		4	23.255	0.0010	24.073	0.0223	26.340	0.0387	29.638	0.0439
	(1,2)	1	44.167	0.0003	45.442	0.0088	48.868	0.0122	53.576	0.0180
		4	29.555	0.0007	31.171	0.0139	35.527	0.0238	41.636	0.0287
	(2,2)	1	72.972	0.0002	73.914	0.0065	76.553	0.0087	80.424	0.0143
		4	48.821	0.0003	50.238	0.0106	54.234	0.0163	60.209	0.0204

Figs 2-6 depict the variations of the first natural frequency ($m = n = 1$) versus the nonlocal factor for different boundary conditions (SSSS, SSCS, CSCS, CCCS and CCCC), electric field strengths, the CNTs distributions and CNT volume fractions, when $h_1 = h_3 = 1$ nm, $\frac{h_2}{h_1} = 1, H_x = 0, L_x = L_y = 10$ nm. It is obvious that the natural frequency for CCCC boundary conditions is generally higher than SSSS boundary conditions because clamped edges are stiffer than simply supported edges. When a sandwich nanoplate is clamped on all four sides, the edges cannot move, and this results in higher stiffness compared to the simply supported edges. As a result, the natural frequency of vibration of the sandwich nanoplate with CCCC boundary conditions is higher than the natural frequency of vibration of the sandwich nanoplate with SSSS boundary conditions. The natural frequency is seen to decrease as the nonlocal parameter increases, which is mostly attributed to the softening effect on this parameter in such small-scale structures. The nonlocal parameter in this context refers to the length scale parameter that accounts for the effects of small-scale phenomena on the behavior of the sandwich nanoplate. As the nonlocal parameter increases, the effects of small-scale phenomena become more pronounced, and the behavior of the nanoplate deviates from classical mechanics. Specifically, the higher-order terms in the governing equations become more significant, which affects the natural frequency of the nanoplate. This means that as the nonlocal parameter increases, the natural frequency decreases. This is because the higher-order terms in the governing equations that become more significant with increasing nonlocality introduce additional stiffness and mass to the nanoplate, which lowers its natural frequency. Moreover, via raising the nonlocal term, the effects of the boundary conditions on the natural frequency decrease. Furthermore, as shown in Figs. 2-6, for the boundary conditions of CCCC, the influences of the electric field on the frequency variations are greater than the SSSS case. As well, it should be stated that the reason behind the higher natural frequency via raising volume fraction is the larger resulting CNTRC stiffness.

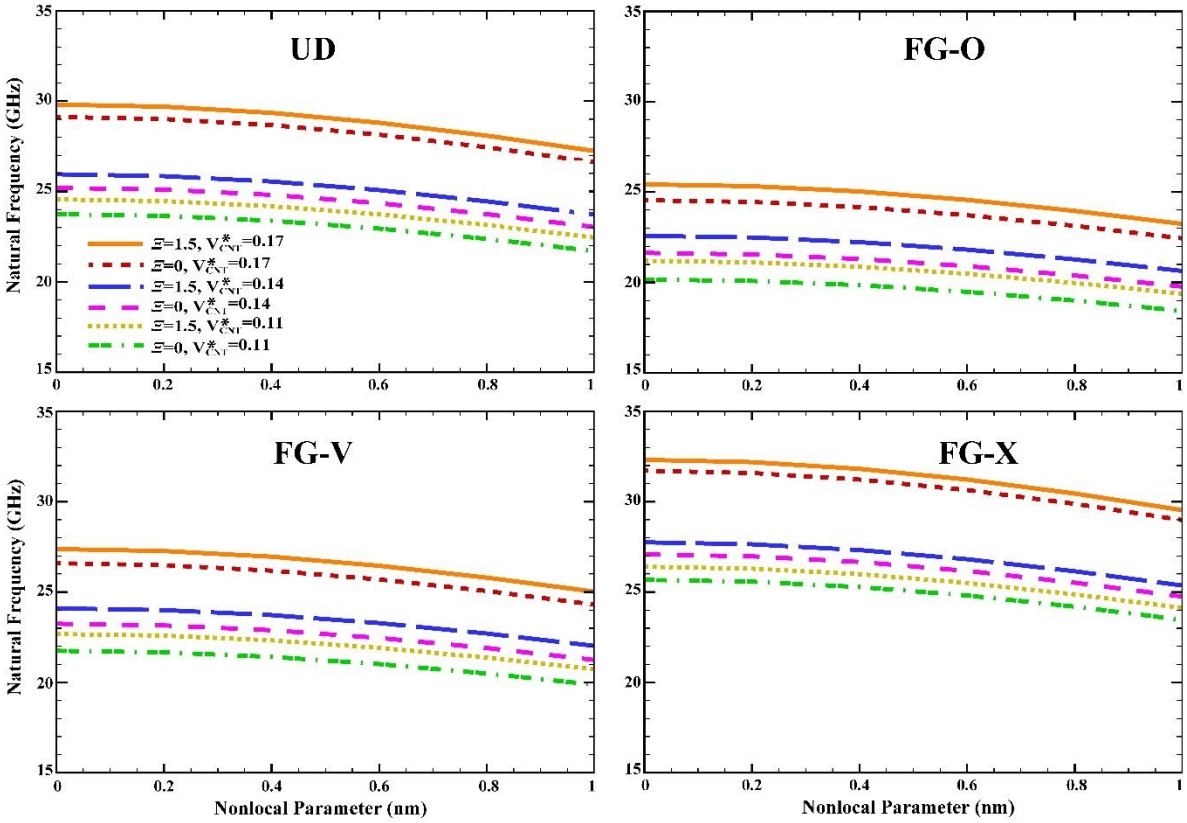

Fig. 2. The effects of the nonlocal parameter, electric field strengths, the CNTs distributions and CNT volume fractions on the variations of the first natural frequency (SSSS).

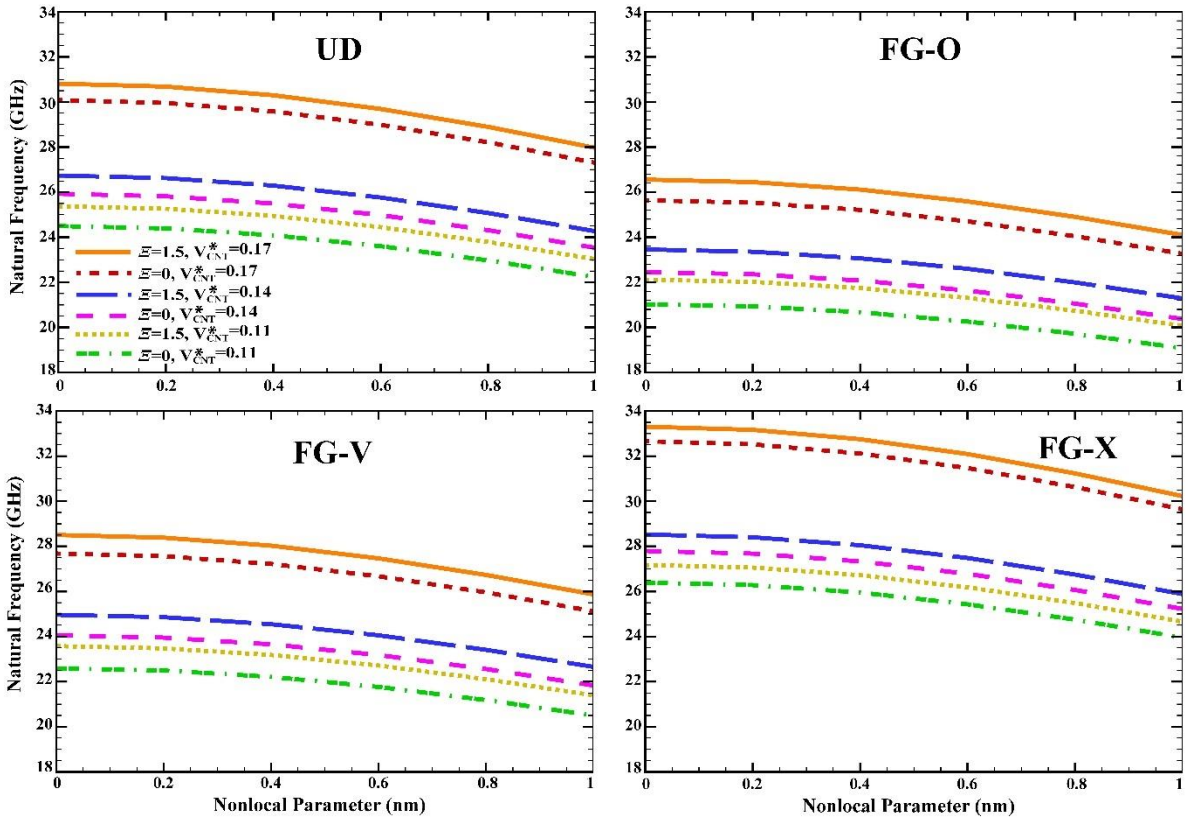

Fig. 3. The effects of the nonlocal parameter, electric field strengths, the CNTs distributions and CNT volume fractions on the variations of the first natural frequency (SSCS).

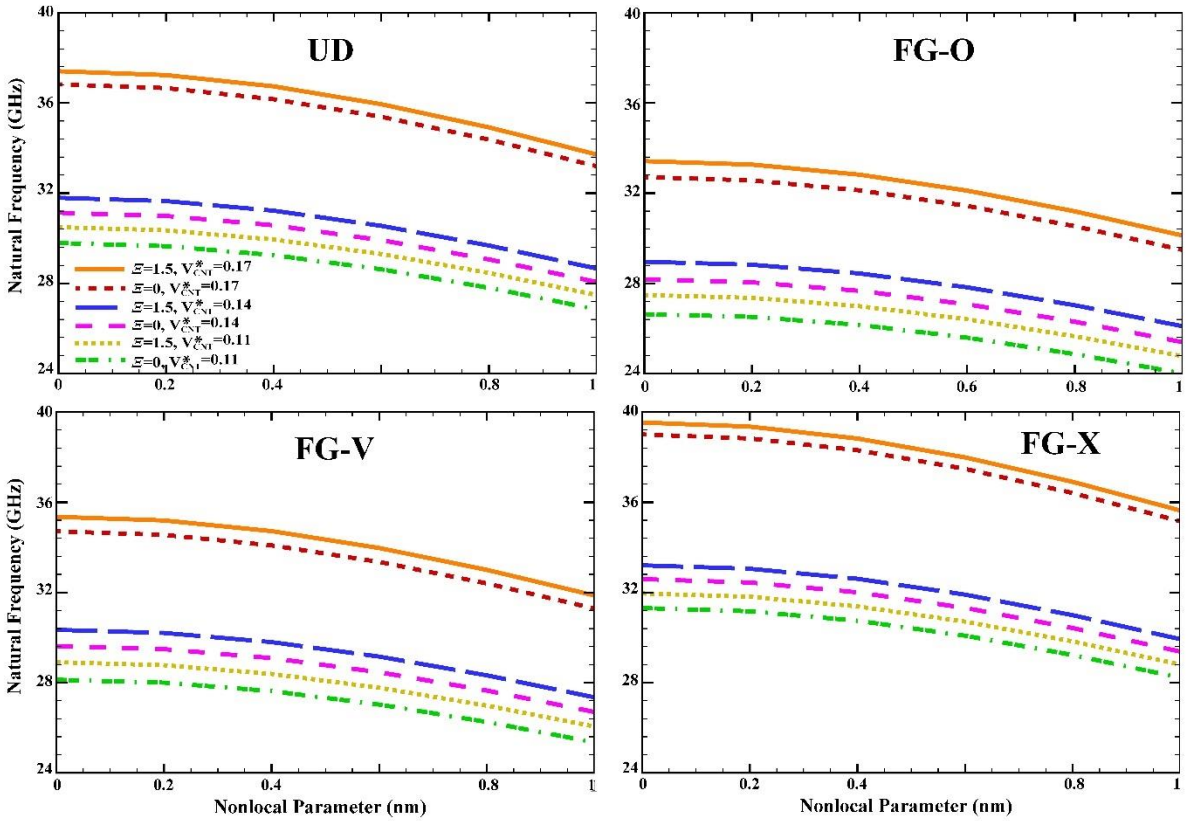

Fig. 4. The effects of the nonlocal parameter, electric field strengths, the CNTs distributions and CNT volume fractions on the variations of the first natural frequency (CSCS).

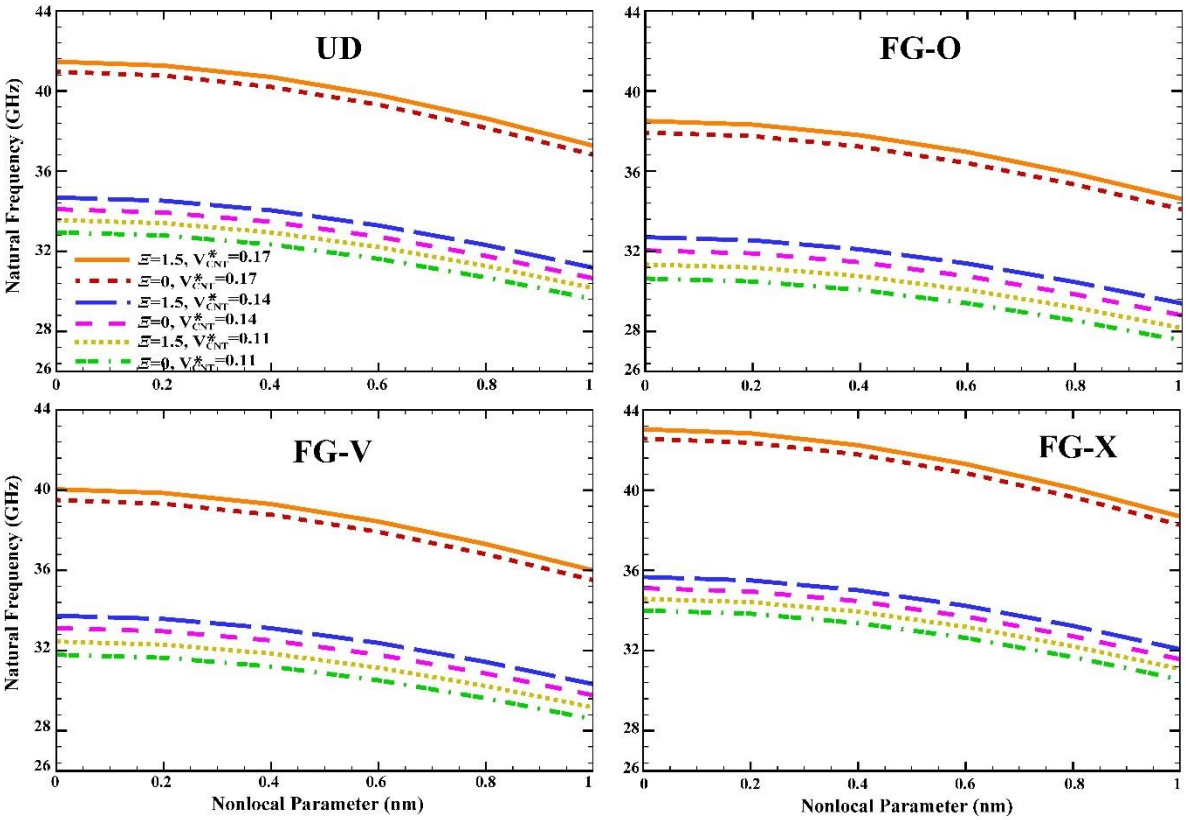

Fig. 5. The effects of the nonlocal parameter, electric field strengths, the CNTs distributions and CNT volume fractions on the variations of the first natural frequency (CCCS).

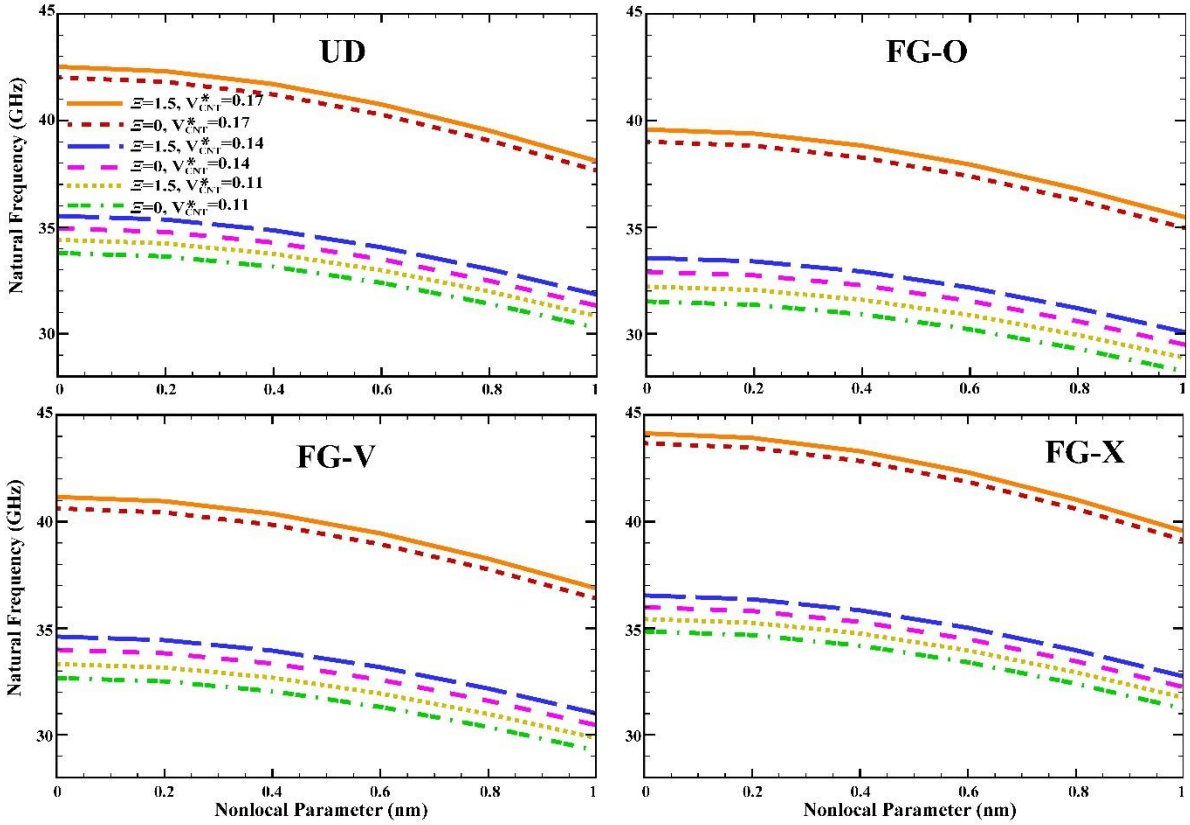

Fig. 6. The effects of the nonlocal parameter, electric field strengths, the CNTs distributions and CNT volume fractions on the variations of the first natural frequency (CCCC).

Fig. 7 illustrates how the thickness ratio, the CNTs' distribution, and the electric field affect variations in the natural frequency for the case of SSSS, when $h_1 = h_3 = 1$ nm, $L_x = L_y = 10$ nm, $H_x = 0, e_0a = 0, V^*_{CNT} = 0.11, m = n = 1$. As seen in Fig. 7, by raising the thickness ratio value $(\frac{h_2}{h_1})$, the system's natural frequency is greatly reduced. This behavior is due to the fact that $\frac{h_2}{h_1}$ has a softening influence on the structure's stiffness, because of the reduction of the total elasticity modulus. The ERF layer and FG-CNTRC layer are two key components that affect the natural frequency of a sandwich plate. The ERF layer is a special fluid that changes its rheological properties (viscosity, stiffness) when an electric field is applied, while the elastic layer is a solid material that provides the sandwich plate's stiffness. Furthermore, the ERF layer also affects the damping of the sandwich plate. Damping is a measure of the ability of the sandwich nanoplate to dissipate energy in response to mechanical loads. As the ERF thickness is increased, the damping of the sandwich nanoplate also increases. This increase in damping leads to a further decrease in the natural frequency of the sandwich plate. When an electric field is applied to an ERF sandwich nanoplate, the fluid undergoes a change in its nanostructure, which results in an increase in its stiffness and natural frequency. The nanostructure of an ERF consists of dispersed particles that are suspended in a carrier fluid. When an electric field is applied, the particles align themselves in the direction of the field, creating chain-like structures called "electrorheological chains." These chains increase the stiffness of the fluid, which in turn increases the natural frequency of the sandwich plate.

Furthermore, it is evident that for a constant value of the ERF electric field, the impact of the various kinds of the CNTs distribution on the natural frequency decreases by increasing $\frac{h_2}{h_1}$. This point is also true for the ERF electric field. Thus, the influence of the various kinds of the CNTs distribution on the variation of the natural frequency decreases when the electric field becomes stronger.

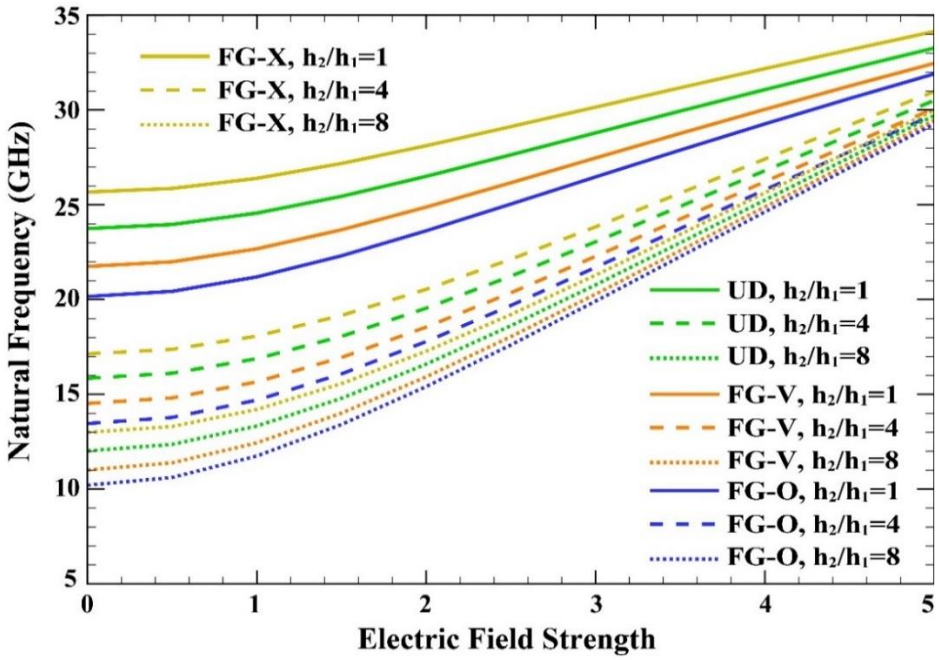

Fig. 7. The effects of the thickness ratio, electric field strengths and CNTs distributions on the variations of the first natural frequency.

Finally, Fig. 8 depicts the influences of magnetic field strength and the CNTs distributions on the change in natural frequency of the sandwich nanoplate for the case of SSSS when $h_1 = h_3 = 1$ nm, $\frac{h_2}{h_1} = 1, \Xi = 0, L_x = L_y = 10$ nm, $V_{CNT}^* = 0.11, m = n = 1$. Longitudinal magnetic fields have a stiffening effect on a structure, as seen in the figure, which causes the fundamental frequency to rise. When a sandwich nanoplate is placed in a longitudinal magnetic field, it experiences a Lorentz force that is proportional to the strength of the magnetic field and the current flowing through the sandwich nanoplate. This Lorentz force causes the sandwich nanoplate to vibrate in a particular mode, and the natural frequency of this vibration mode is proportional to the Lorentz force. Therefore, as the longitudinal magnetic field is increased, the Lorentz force on the nanoplate increases, which causes the natural frequency of its vibration mode to increase. This effect can be useful in applications where precise control of the natural frequency of a sandwich nanoplate is required, such as in nanomechanical resonators used for sensing and measurement.

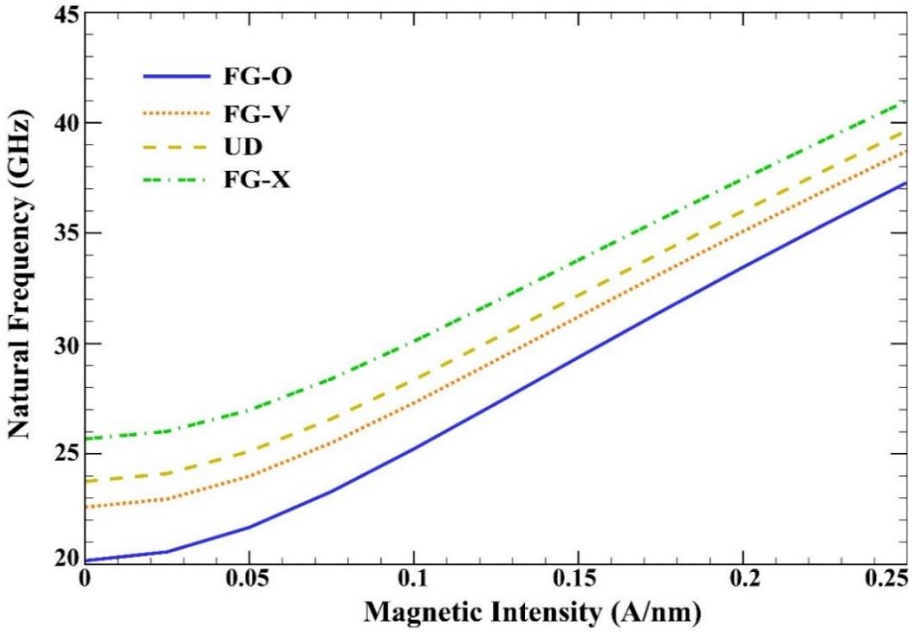

Fig. 8. The effects of the longitudinal magnetic field strength and the CNTs distributions on the change in the first natural frequency.

5. Conclusions

In this study, the free vibration problem of an FG-CNTRC sandwich nanoplate with ERF core layer under longitudinal magnetic field has been analytically examined using TSDT and nonlocal elasticity theory. In TSDT, the plate is assumed to deform in three directions: two in-plane translations and one out-of-plane rotation. This allows for the consideration of transverse shear deformations that are not accounted for in lower-order theories, such as the classical plate theory and the FSDT. All layers of the sandwich plate must maintain physical continuity, and the rule of mixing allows us to examine how mechanical characteristics are distributed in the thickness direction of this system. In order to solve the resulting equations, the Galerkin method is employed. Parameter investigations demonstrate the influences of the ERF electric field, boundary conditions, CNTs distributions, CNT volume fraction, and nonlocal parameter on the free vibration. Following are some noteworthy conclusions that may be derived from the results:

- The geometric thickness ratio value controls how much the electric field affects the modal loss factor. It appears that the loss factor grows at small electric fields, then it peaks at a medium electric field, and finally decreases at higher values of electric field intensity.

- The structural stiffness is strongly dependent upon the CNTs distribution. Natural frequencies' smallest and greatest ranges are exhibited by FG-O and FG-X distributions, respectively.
- The thickness ratio ($\frac{h_2}{h_1}$) strongly affects the natural frequency of an FG-CNTRC sandwich nanoplate with ERF core layer. This study also provides valuable insight into the potential applications of CNTs, including the structural parts of different sensors and nanodevices.

- Longitudinal magnetic fields have a stiffening effect on a structure, which causes the natural frequency to rise.
- The natural frequency is seen to decrease as the nonlocal parameter increases, which is mostly attributed to the softening effect on this parameter in such small-scale structures.
- Via raising $\frac{h_2}{h_1}$ and ERF electric field, the influence of the various categories of the CNTs distribution on the natural frequency decreases.
- The natural frequency for CCCC boundary conditions is generally higher than SSSS boundary conditions because clamped edges are stiffer than simply supported edges.

APPENDIX A

The governing equations of the sandwich nanoplate are provided as

$$\delta u_{0t} \rightarrow \frac{\partial N_{xx}^{t}}{\partial x}+\frac{\partial N_{xy}^{t}}{\partial y}-\frac{3Q_{xz}^{c}}{4h_2}+\frac{9C_1R_{xz}^{c}}{4h_2}=I_0^{t}\ddot{u}_{0t}+\bar{I}_1^{t}\ddot{\theta}_{xt}-I_3^{t}C_1\frac{\partial \ddot{W}_0}{\partial x}, \tag{A1}$$

$$\delta u_{0b} \rightarrow \frac{\partial N_{xx}^{b}}{\partial x}+\frac{\partial N_{xy}^{b}}{\partial y}+\frac{3Q_{xz}^{c}}{4h_2}-\frac{9C_1R_{xz}^{c}}{4h_2}=I_0^{b}\ddot{u}_{0b}+\bar{I}_1^{b}\ddot{\theta}_{xb}-I_3^{b}C_1\frac{\partial \ddot{W}_0}{\partial x}, \tag{A2}$$

$$\delta v_{0t} \rightarrow \frac{\partial N_{yy}^{t}}{\partial y}+\frac{\partial N_{xy}^{t}}{\partial x}-\frac{3Q_{yz}^{c}}{4h_2}+\frac{9C_1R_{yz}^{c}}{4h_2}=I_0^{t}\ddot{v}_{0t}+\bar{I}_1^{t}\ddot{\theta}_{yt}-I_3^{t}C_1\frac{\partial \ddot{W}_0}{\partial y}, \tag{A3}$$

$$\delta v_{0b} \rightarrow \frac{\partial N_{yy}^{b}}{\partial y}+\frac{\partial N_{xy}^{b}}{\partial x}+\frac{3Q_{yz}^{c}}{4h_2}-\frac{9C_1R_{yz}^{c}}{4h_2}=I_0^{b}\ddot{v}_{0b}+\bar{I}_1^{b}\ddot{\theta}_{yb}-I_3^{b}C_1\frac{\partial \ddot{W}_0}{\partial y}, \tag{A4}$$

$$\begin{aligned}\delta W_0 \rightarrow{}& \frac{\partial Q_{xz}^{t}}{\partial x}+\frac{\partial Q_{xz}^{b}}{\partial x}+\frac{\partial Q_{yz}^{t}}{\partial y}+\frac{\partial Q_{yz}^{b}}{\partial y}-3C_1\left(\frac{\partial R_{xz}^{t}}{\partial x}+\frac{\partial R_{yz}^{t}}{\partial y}\right)-3C_1\left(\frac{\partial R_{xz}^{b}}{\partial x}+\frac{\partial R_{yz}^{b}}{\partial y}\right)+\\ &C_1\left(\frac{\partial^2 P_{xx}^{t}}{\partial x^2}+2\frac{\partial^2 P_{xy}^{t}}{\partial x\partial y}+\frac{\partial^2 P_{yy}^{t}}{\partial y^2}\right)+C_1\left(\frac{\partial^2 P_{xx}^{b}}{\partial x^2}+2\frac{\partial^2 P_{xy}^{b}}{\partial x\partial y}+\frac{\partial^2 P_{yy}^{b}}{\partial y^2}\right)+\left(\frac{3}{4}-\frac{h_1}{8h_2}-\right.\\ &\left.\frac{h_3}{8h_2}\right)\left(\frac{\partial Q_{xz}^{c}}{\partial x}+\frac{\partial Q_{yz}^{c}}{\partial y}\right)-\left(\frac{9}{4}-\frac{3h_1}{8h_2}-\frac{3h_3}{8h_2}\right)C_1\left(\frac{\partial R_{xz}^{c}}{\partial x}+\frac{\partial R_{yz}^{c}}{\partial y}\right)=q+\left(I_0^{t}+I_0^{c}+I_0^{b}\right)\ddot{W}_0+\\ &I_3^{t}C_1\left(\frac{\partial \ddot{u}_{0t}}{\partial x}+\frac{\partial \ddot{v}_{0t}}{\partial y}\right)+I_3^{b}C_1\left(\frac{\partial \ddot{u}_{0b}}{\partial x}+\frac{\partial \ddot{v}_{0b}}{\partial y}\right)-\left(I_6^{t}+I_3^{b}\right)C_1^{2}\left(\frac{\partial^2 \ddot{W}_0}{\partial x^2}+\frac{\partial^2 \ddot{W}_0}{\partial y^2}\right)+\\ &\bar{I}_4^{t}C_1\left(\frac{\partial \ddot{\theta}_{xt}}{\partial x}+\frac{\partial \ddot{\theta}_{yt}}{\partial y}\right)+\bar{I}_4^{b}C_1\left(\frac{\partial \ddot{\theta}_{xb}}{\partial x}+\frac{\partial \ddot{\theta}_{yb}}{\partial y}\right),\end{aligned} \tag{A5}$$

$$\delta\theta_{xt} \rightarrow \frac{\partial M_{xx}^{t}}{\partial x}+\frac{\partial M_{xy}^{t}}{\partial y}-C_1\left(\frac{\partial P_{xx}^{t}}{\partial x}+\frac{\partial P_{xy}^{t}}{\partial y}\right)-Q_{xz}^{t}+3C_1R_{xz}^{t}+\frac{h_1Q_{xz}^{c}}{2h_2}-\frac{3C_1h_1R_{xz}^{c}}{2h_2}=\bar{I}_1^{t}\ddot{u}_{0t}+\bar{I}_2^{t}\ddot{\theta}_{xt}-C_1\bar{I}_4^{t}\frac{\partial \ddot{W}_0}{\partial x}, \tag{A6}$$

$$\delta\theta_{xb} \rightarrow \frac{\partial M_{xx}^{b}}{\partial x}+\frac{\partial M_{xy}^{b}}{\partial y}-C_1\left(\frac{\partial P_{xx}^{b}}{\partial x}+\frac{\partial P_{xy}^{b}}{\partial y}\right)-Q_{xz}^{b}+3C_1R_{xz}^{b}+\frac{h_3Q_{xz}^{c}}{2h_2}-\frac{3C_1h_3R_{xz}^{c}}{2h_2}=\bar{I}_1^{b}\ddot{u}_{0b}+\bar{I}_2^{b}\ddot{\theta}_{xb}-C_1\bar{I}_4^{b}\frac{\partial \ddot{W}_0}{\partial x}, \tag{A7}$$

$$\delta\theta_{yt} \rightarrow \frac{\partial M_{yy}^{t}}{\partial y}+\frac{\partial M_{xy}^{t}}{\partial x}-C_1\left(\frac{\partial P_{yy}^{t}}{\partial y}+\frac{\partial P_{xy}^{t}}{\partial x}\right)-Q_{yz}^{t}+3C_1R_{yz}^{t}+\frac{h_1Q_{yz}^{c}}{2h_2}-\frac{3C_1h_1R_{yz}^{c}}{2h_2}=\bar{I}_1^{t}\ddot{v}_{0t}+\bar{I}_2^{t}\ddot{\theta}_{yt}-C_1\bar{I}_4^{t}\frac{\partial \ddot{W}_0}{\partial y}, \tag{A8}$$

$$\delta\theta_{yb} \rightarrow \frac{\partial M_{yy}^b}{\partial y} + \frac{\partial M_{xy}^b}{\partial x} - C_1\left(\frac{\partial P_{yy}^b}{\partial y} + \frac{\partial P_{xy}^b}{\partial x}\right) - Q_{yz}^t + 3C_1R_{yz}^b + \frac{h_3Q_{yz}^c}{2h_2} - \frac{3C_1h_3R_{yz}^c}{2h_2} = \bar{I}_1^b\ddot{v}_{0b} + \bar{I}_2^b\ddot{\theta}_{yb} - C_1\bar{I}_4^b\frac{\partial\ddot{W}_0}{\partial y}, \quad \text{(A9)}$$

where

$$(I_0^t, I_1^t, I_2^t, I_3^t, I_4^t, I_6^t) = \int_{-h_1/2}^{h_1/2}\rho(1, z, z^2, z^3, z^4, z^6)dz,$$

$$\left(I_0^b, I_1^b, I_2^b, I_3^b, I_4^b, I_6^b\right) = \int_{-h_3/2}^{h_3/2}\rho(1, z, z^2, z^3, z^4, z^6)dz,\ I_0^c = \int_{-h_2/2}^{h_2/2}\rho_f dz, \quad \text{(A10)}$$

$$\bar{I}_1^t = I_1^t - I_3^tC_1,\ \bar{I}_2^t = I_2^t - 2C_1I_4^t + C_1^2I_6^t,\ \bar{I}_4^t = I_4^t - C_1I_6^t,$$

$$\bar{I}_1^b = I_1^b - I_3^bC_1,\ \bar{I}_2^b = I_2^b - 2C_1I_4^b + C_1^2I_6^b,\ \bar{I}_4^b = I_4^b - C_1I_6^b,$$

$$(N_{xx}^t, M_{xx}^t, P_{xx}^t) = \int_{-h_1/2}^{h_1/2}\sigma_{xxt}(1, z, z^3)dz,$$

$$\left(N_{xy}^t, M_{xy}^t, P_{xy}^t\right) = \int_{-h_1/2}^{h_1/2}\tau_{xyt}(1, z, z^3)dz,$$

$$\left(N_{yy}^t, M_{yy}^t, P_{yy}^t\right) = \int_{-h_1/2}^{h_1/2}\sigma_{yyt}(1, z, z^3)dz,$$

$$(Q_{xz}^t, R_{xz}^t) = \int_{-h_1/2}^{h_1/2}\tau_{xzt}(1, z^2)dz,\ \ (Q_{xz}^t, R_{xz}^t) = \int_{-h_1/2}^{h_1/2}\tau_{xzt}(1, z^2)dz,$$

$$(N_{xx}^b, M_{xx}^b, P_{xx}^b) = \int_{-h_3/2}^{h_3/2}\sigma_{xxb}(1, z, z^3)dz,$$

$$\left(N_{xy}^b, M_{xy}^b, P_{xy}^b\right) = \int_{-h_3/2}^{h_3/2}\tau_{xyb}(1, z, z^3)dz,$$

$$\left(N_{yy}^b, M_{yy}^b, P_{yy}^b\right) = \int_{-h_3/2}^{h_3/2}\sigma_{yyb}(1, z, z^3)dz,$$

$$(Q_{xz}^b, R_{xz}^b) = \int_{-h_3/2}^{h_3/2}\tau_{xzb}(1, z^2)dz,\ \ (Q_{xz}^b, R_{xz}^b) = \int_{-h_3/2}^{h_3/2}\tau_{xzb}(1, z^2)dz,$$

$$(Q_{xz}^c, R_{xz}^c) = \int_{-h_2/2}^{h_2/2}\tau_{xzc}(1, z^2)dz, \left(Q_{yz}^c, R_{yz}^c\right) = \int_{-h_2/2}^{h_2/2}\tau_{yzc}(1, z^2)dz.$$

APPENDIX B

The size-dependent governing partial differential equations are provided as

$$\delta u_{0t} \rightarrow A_{11}\left(\frac{\partial^2 u_{0t}}{\partial x^2}\right) + A_{66}\left(\frac{\partial^2 u_{0t}}{\partial y^2}\right) + [A_{12} + A_{66}]\left(\frac{\partial^2 v_{0t}}{\partial x\partial y}\right) + [B_{11} - C_1E_{11}]\left(\frac{\partial^2\theta_{xt}}{\partial x^2}\right) + [B_{66} - C_1E_{66}]\left(\frac{\partial^2\theta_{xt}}{\partial y^2}\right) + [B_{12} + B_{66} - C_1E_{12} - C_1E_{66}]\left(\frac{\partial^2\theta_{yt}}{\partial x\partial y}\right) - [C_1E_{12} + 2C_1E_{66}]\left(\frac{\partial^3 W_0}{\partial x\partial y^2}\right) - C_1E_{11}\left(\frac{\partial^3 W_0}{\partial x^3}\right) - \left(\frac{3}{4h_2}f_1 - \frac{9}{4h_2}C_1f_4\right)(u_{0t} - u_{0b}) + \left(\frac{3}{4h_2}f_2 - \frac{9}{4h_2}C_1f_5\right)(h_1\theta_{xt} + h_3\theta_{xb}) + \left(\frac{3}{4h_2}f_3 - \frac{9}{4h_2}C_1f_6\right)\frac{\partial W_0}{\partial x} = [1 - (e_0a)^2\nabla^2]\left(I_0^t\ddot{u}_{0t} + \bar{I}_1^t\ddot{\theta}_{xt} - I_3^tC_1\frac{\partial\ddot{W}_0}{\partial x}\right), \quad \text{(B1)}$$

$$\delta u_{0b} \rightarrow A_{11}\left(\frac{\partial^2 u_{0b}}{\partial x^2}\right) + A_{66}\left(\frac{\partial^2 u_{0b}}{\partial y^2}\right) + [A_{12} + A_{66}]\left(\frac{\partial^2 v_{0b}}{\partial x\partial y}\right) + [B_{11} - C_1E_{11}]\left(\frac{\partial^2\theta_{xb}}{\partial x^2}\right) + [B_{66} - C_1E_{66}]\left(\frac{\partial^2\theta_{xb}}{\partial y^2}\right) + [B_{12} + B_{66} - C_1E_{12} -$$

$$C_1E_{66}]\left(\frac{\partial^2\theta_{yb}}{\partial x\partial y}\right)-[C_1E_{12}+2C_1E_{66}]\left(\frac{\partial^3W_0}{\partial x\partial y^2}\right)-C_1E_{11}\left(\frac{\partial^3W_0}{\partial x^3}\right)+\left(\frac{3}{4h_2}f_1-\frac{9}{4h_2}C_1f_4\right)(u_{0t}-u_{0b})-\left(\frac{3}{4h_2}f_2-\frac{9}{4h_2}C_1f_5\right)(h_1\theta_{xt}+h_3\theta_{xb})-\left(\frac{3}{4h_2}f_3-\frac{9}{4h_2}C_1f_6\right)\frac{\partial W_0}{\partial x}=[1-(e_0a)^2\nabla^2]\left(I_0^b\ddot{u}_{0b}+\bar{I}_1^b\ddot{\theta}_{xb}-I_3^bC_1\frac{\partial\ddot{W}_0}{\partial x}\right),$$ (B2)

$$\delta v_{0t}\rightarrow A_{22}\left(\frac{\partial^2v_{0t}}{\partial y^2}\right)+A_{66}\left(\frac{\partial^2v_{0t}}{\partial x^2}\right)+[A_{21}+A_{66}]\left(\frac{\partial^2u_{0t}}{\partial x\partial y}\right)+[B_{66}-C_1E_{66}]\left(\frac{\partial^2\theta_{yt}}{\partial x^2}\right)+[B_{22}-C_1E_{22}]\left(\frac{\partial^2\theta_{yt}}{\partial y^2}\right)+[B_{21}+B_{66}-C_1E_{21}-C_1E_{66}]\left(\frac{\partial^2\theta_{xt}}{\partial x\partial y}\right)-[C_1E_{21}+2C_1E_{66}]\left(\frac{\partial^3W_0}{\partial x^2\partial y}\right)-C_1E_{22}\left(\frac{\partial^3W_0}{\partial y^3}\right)-\left(\frac{3}{4h_2}f_1-\frac{9}{4h_2}C_1f_4\right)(v_{0t}-v_{0b})+\left(\frac{3}{4h_2}f_2-\frac{9}{4h_2}C_1f_5\right)(h_1\theta_{yt}+h_3\theta_{yb})+\left(\frac{3}{4h_2}f_3-\frac{9}{4h_2}C_1f_6\right)\frac{\partial W_0}{\partial y}=[1-(e_0a)^2\nabla^2]\left(I_0^t\ddot{v}_{0t}+\bar{I}_1^t\ddot{\theta}_{yt}-I_3^tC_1\frac{\partial\ddot{W}_0}{\partial y}\right),$$ (B3)

$$v_{0b}\rightarrow A_{22}\left(\frac{\partial^2v_{0b}}{\partial y^2}\right)+A_{66}\left(\frac{\partial^2v_{0b}}{\partial x^2}\right)+[A_{21}+A_{66}]\left(\frac{\partial^2u_{0b}}{\partial x\partial y}\right)+[B_{66}-C_1E_{66}]\left(\frac{\partial^2\theta_{yb}}{\partial x^2}\right)+[B_{22}-C_1E_{22}]\left(\frac{\partial^2\theta_{yb}}{\partial y^2}\right)+[B_{21}+B_{66}-C_1E_{21}-C_1E_{66}]\left(\frac{\partial^2\theta_{xb}}{\partial x\partial y}\right)-[C_1E_{21}+2C_1E_{66}]\left(\frac{\partial^3W_0}{\partial x^2\partial y}\right)-C_1E_{22}\left(\frac{\partial^3W_0}{\partial y^3}\right)+\left(\frac{3}{4h_2}f_1-\frac{9}{4h_2}C_1f_4\right)(v_{0t}-v_{0b})-\left(\frac{3}{4h_2}f_2-\frac{9}{4h_2}C_1f_5\right)(h_1\theta_{yt}+h_3\theta_{yb})-\left(\frac{3}{4h_2}f_3-\frac{9}{4h_2}C_1f_6\right)\frac{\partial W_0}{\partial y}=[1-(e_0a)^2\nabla^2]\left(I_0^t\ddot{v}_{0t}+\bar{I}_1^t\ddot{\theta}_{yt}-I_3^tC_1\frac{\partial\ddot{W}_0}{\partial y}\right),$$ (B4)

$$\delta W_0\rightarrow 2[A_{44}-6C_1H_{44}+9C_1^2T_{44}]\left(\frac{\partial^2W_0}{\partial x^2}+\frac{\partial^2W_0}{\partial y^2}\right)+[A_{44}-6C_1H_{44}+9C_1^2T_{44}]\left(\frac{\partial\theta_{xt}}{\partial x}+\frac{\partial\theta_{yt}}{\partial y}+\frac{\partial\theta_{xb}}{\partial x}+\frac{\partial\theta_{yb}}{\partial y}\right)+C_1E_{11}\left(\frac{\partial^3u_{0t}}{\partial x^3}+\frac{\partial^3u_{0b}}{\partial x^3}\right)+C_1E_{22}\left(\frac{\partial^3v_{0t}}{\partial y^3}+\frac{\partial^3v_{0b}}{\partial y^3}\right)+[C_1E_{12}+2C_1E_{66}]\left(\frac{\partial^3u_{0t}}{\partial x\partial y^2}+\frac{\partial^3u_{0b}}{\partial x\partial y^2}+\frac{\partial^3v_{0t}}{\partial x^2\partial y}+\frac{\partial^3v_{0b}}{\partial x^2\partial y}\right)+[C_1T_{11}-C_1^2D_{11}]\left(\frac{\partial^3\theta_{xt}}{\partial x^3}+\frac{\partial^3\theta_{xt}}{\partial x^3}\right)+[C_1T_{22}-C_1^2D_{22}]\left(\frac{\partial^3\theta_{yt}}{\partial y^3}+\frac{\partial^3\theta_{yb}}{\partial y^3}\right)+[C_1T_{12}-C_1^2D_{12}+2(C_1T_{66}-C_1^2D_{66})]\left(\frac{\partial^3\theta_{xt}}{\partial x\partial y^2}+\frac{\partial^3\theta_{yt}}{\partial x^2\partial y}+\frac{\partial^3\theta_{xb}}{\partial x\partial y^2}+\frac{\partial^3\theta_{yb}}{\partial x^2\partial y}\right)-2C_1^2D_{11}\left(\frac{\partial^4W_0}{\partial x^4}\right)-2C_1^2D_{22}\left(\frac{\partial^4W_0}{\partial y^4}\right)-2[2C_1^2D_{12}+4C_1^2D_{66}]\left(\frac{\partial^4W_0}{\partial x^2\partial y^2}\right)-(rf_1-rC_1f_4)\left(\frac{\partial u_{0t}}{\partial x}-\frac{\partial u_{0b}}{\partial x}\right)+(rf_2-rC_1f_5)\left(h_1\frac{\partial\theta_{xt}}{\partial x}+h_2\frac{\partial\theta_{xb}}{\partial x}\right)+(rf_3-rC_1f_6)\frac{\partial^2W_0}{\partial x^2}-(rf_1-rC_1f_4)\left(\frac{\partial v_{0t}}{\partial y}-\frac{\partial v_{0b}}{\partial x}\right)+(rf_2-rC_1f_5)\left(h_1\frac{\partial\theta_{yt}}{\partial y}+h_2\frac{\partial\theta_{yb}}{\partial y}\right)+(rf_3-rC_1f_6)\frac{\partial^2W_0}{\partial y^2}=[1-(e_0a)^2\nabla^2]\left\{q+\left(I_0^t+I_0^c+I_0^b\right)\ddot{W}_0+I_3^tC_1\left(\frac{\partial\ddot{u}_{0t}}{\partial x}+\frac{\partial\ddot{v}_{0t}}{\partial y}\right)+I_3^bC_1\left(\frac{\partial\ddot{u}_{0b}}{\partial x}+\frac{\partial\ddot{v}_{0b}}{\partial y}\right)-\left(I_6^t+I_3^b\right)C_1^2\left(\frac{\partial^2\ddot{W}_0}{\partial x^2}+\frac{\partial^2\ddot{W}_0}{\partial y^2}\right)+\bar{I}_4^tC_1\left(\frac{\partial\ddot{\theta}_{xt}}{\partial x}+\frac{\partial\ddot{\theta}_{yt}}{\partial y}\right)+\bar{I}_4^bC_1\left(\frac{\partial\ddot{\theta}_{xb}}{\partial x}+\frac{\partial\ddot{\theta}_{yb}}{\partial y}\right)\right\},$$ (B5)

$$\delta\theta_{xt}\rightarrow[B_{11}-C_1E_{11}]\left(\frac{\partial^2u_{0t}}{\partial x^2}\right)+[B_{66}-C_1E_{66}]\left(\frac{\partial^2u_{0t}}{\partial y^2}\right)+[B_{12}-C_1E_{12}+B_{66}-C_1E_{66}]\left(\frac{\partial^2v_{0t}}{\partial x\partial y}\right)+[H_{11}-2C_1T_{11}+C_1^2D_{11}]\left(\frac{\partial^2\theta_{xt}}{\partial x^2}\right)+[H_{66}-2C_1T_{66}+C_1^2D_{66}]\left(\frac{\partial^2\theta_{xt}}{\partial y^2}\right)+[H_{12}-2C_1T_{12}+H_{66}-2C_1T_{66}+C_1^2D_{12}+C_1^2D_{66}]\left(\frac{\partial^2\theta_{yt}}{\partial x\partial y}\right)+[6C_1H_{44}-A_{44}-9C_1^2T_{44}]\left(\theta_{xt}+\frac{\partial W_0}{\partial x}\right)+(C_1^2D_{11}-C_1T_{11})\left(\frac{\partial^3W_0}{\partial x^3}\right)+[C_1^2D_{12}-C_1T_{12}+2(C_1^2D_{66}-C_1T_{66})]\left(\frac{\partial^3W_0}{\partial x\partial y^2}\right)+\left(\frac{h_1}{2h_2}f_1-\frac{3C_1h_1}{2h_2}f_4\right)(u_{0t}-u_{0b})-$$ (B6)

$$\left(\frac{h_1}{2h_2}f_2-\frac{3C_1h_1}{2h_2}f_5\right)(h_1\theta_{xt}+h_3\theta_{xb})-\left(\frac{h_1}{2h_2}f_3-\frac{3C_1h_1}{2h_2}f_6\right)\frac{\partial W_0}{\partial x}=[1-(e_0a)^2\nabla^2]\left(\bar{I}_1^t\ddot{u}_{0t}+\bar{I}_2^t\ddot{\theta}_{xt}-C_1\bar{I}_4^t\frac{\partial\ddot{W}_0}{\partial x}\right),$$

$$\delta\theta_{xb}\rightarrow[B_{11}-C_1E_{11}]\left(\frac{\partial^2u_{0b}}{\partial x^2}\right)+[B_{66}-C_1E_{66}]\left(\frac{\partial^2u_{0b}}{\partial y^2}\right)+[B_{12}-C_1E_{12}+B_{66}-C_1E_{66}]\left(\frac{\partial^2v_{0b}}{\partial x\partial y}\right)+[H_{11}-2C_1T_{11}+C_1^2D_{11}]\left(\frac{\partial^2\theta_{xb}}{\partial x^2}\right)+[H_{66}-2C_1T_{66}+C_1^2D_{66}]\left(\frac{\partial^2\theta_{xb}}{\partial y^2}\right)+[H_{12}-2C_1T_{12}+H_{66}-2C_1T_{66}+C_1^2D_{12}+C_1^2D_{66}]\left(\frac{\partial^2\theta_{yb}}{\partial x\partial y}\right)+[6C_1H_{44}-A_{44}-9C_1^2T_{44}]\left(\theta_{xb}+\frac{\partial W_0}{\partial x}\right)+(C_1^2D_{11}-C_1T_{11})\left(\frac{\partial^3W_0}{\partial x^3}\right)+[C_1^2D_{12}-C_1T_{12}+2(C_1^2D_{66}-C_1T_{66})]\left(\frac{\partial^3W_0}{\partial x\partial y^2}\right)+\left(\frac{h_3}{2h_2}f_1-\frac{3C_1h_3}{2h_2}f_4\right)(u_{0t}-u_{0b})-\left(\frac{h_3}{2h_2}f_2-\frac{3C_1h_3}{2h_2}f_5\right)(h_1\theta_{xt}+h_3\theta_{xb})-\left(\frac{h_3}{2h_2}f_3-\frac{3C_1h_3}{2h_2}f_6\right)\frac{\partial W_0}{\partial x}=[1-(e_0a)^2\nabla^2]\left(\bar{I}_1^b\ddot{u}_{0b}+\bar{I}_2^b\ddot{\theta}_{xb}-C_1\bar{I}_4^b\frac{\partial\ddot{W}_0}{\partial x}\right), \tag{B7}$$

$$\delta\theta_{yt}\rightarrow[B_{22}-C_1E_{22}]\left(\frac{\partial^2v_{0t}}{\partial y^2}\right)+[B_{66}-C_1E_{66}]\left(\frac{\partial^2v_{0t}}{\partial x^2}\right)+[B_{12}-C_1E_{12}+B_{66}-C_1E_{66}]\left(\frac{\partial^2u_{0t}}{\partial x\partial y}\right)+[H_{22}-2C_1T_{22}+C_1^2D_{22}]\left(\frac{\partial^2\theta_{yt}}{\partial y^2}\right)+[H_{66}-2C_1T_{66}+C_1^2D_{66}]\left(\frac{\partial^2\theta_{yt}}{\partial x^2}\right)+[H_{12}-2C_1T_{12}+H_{66}-2C_1T_{66}+C_1^2D_{12}+C_1^2D_{66}]\left(\frac{\partial^2\theta_{xt}}{\partial x\partial y}\right)+[6C_1H_{44}-A_{44}-9C_1^2T_{44}]\left(\theta_{yt}+\frac{\partial W_0}{\partial y}\right)+(C_1^2D_{22}-C_1T_{22})\left(\frac{\partial^3W_0}{\partial y^3}\right)+[C_1^2D_{12}-C_1T_{12}+2(C_1^2D_{66}-C_1T_{66})]\left(\frac{\partial^3W_0}{\partial x^2\partial y}\right)+\left(\frac{h_1}{2h_2}f_1-\frac{3C_1h_1}{2h_2}f_4\right)(v_{0t}-v_{0b})-\left(\frac{h_1}{2h_2}f_2-\frac{3C_1h_1}{2h_2}f_5\right)(h_1\theta_{yt}+h_3\theta_{yb})-\left(\frac{h_1}{2h_2}f_3-\frac{3C_1h_1}{2h_2}f_6\right)\frac{\partial W_0}{\partial y}=[1-(e_0a)^2\nabla^2]\left(\bar{I}_1^t\ddot{v}_{0t}+\bar{I}_2^t\ddot{\theta}_{yt}-C_1\bar{I}_4^t\frac{\partial\ddot{W}_0}{\partial y}\right), \tag{B8}$$

$$\delta\theta_{yb}\rightarrow[B_{22}-C_1E_{22}]\left(\frac{\partial^2v_{0b}}{\partial y^2}\right)+[B_{66}-C_1E_{66}]\left(\frac{\partial^2v_{0b}}{\partial x^2}\right)+[B_{12}-C_1E_{12}+B_{66}-C_1E_{66}]\left(\frac{\partial^2u_{0b}}{\partial x\partial y}\right)+[H_{22}-2C_1T_{22}+C_1^2D_{22}]\left(\frac{\partial^2\theta_{yb}}{\partial y^2}\right)+[H_{66}-2C_1T_{66}+C_1^2D_{66}]\left(\frac{\partial^2\theta_{yb}}{\partial x^2}\right)+[H_{12}-2C_1T_{12}+H_{66}-2C_1T_{66}+C_1^2D_{12}+C_1^2D_{66}]\left(\frac{\partial^2\theta_{xb}}{\partial x\partial y}\right)+[6C_1H_{44}-A_{44}-9C_1^2T_{44}]\left(\theta_{yb}+\frac{\partial W_0}{\partial y}\right)+(C_1^2D_{22}-C_1T_{22})\left(\frac{\partial^3W_0}{\partial y^3}\right)+[C_1^2D_{12}-C_1T_{12}+2(C_1^2D_{66}-C_1T_{66})]\left(\frac{\partial^3W_0}{\partial x^2\partial y}\right)+\left(\frac{h_3}{2h_2}f_1-\frac{3C_1h_3}{2h_2}f_4\right)(v_{0t}-v_{0b})-\left(\frac{h_3}{2h_2}f_2-\frac{3C_1h_3}{2h_2}f_5\right)(h_1\theta_{yt}+h_3\theta_{yb})-\left(\frac{h_3}{2h_2}f_3-\frac{3C_1h_3}{2h_2}f_6\right)\frac{\partial W_0}{\partial y}=[1-(e_0a)^2\nabla^2]\left(\bar{I}_1^b\ddot{v}_{0b}+\bar{I}_2^b\ddot{\theta}_{yb}-C_1\bar{I}_4^b\frac{\partial\ddot{W}_0}{\partial y}\right), \tag{B9}$$

where

$$(A_{11},B_{11},H_{11},E_{11},T_{11},D_{11})=\int_{-h_1/2}^{h_1/2}Q_{11}(1,z,z^2,z^3,z^4,z^6)dz,$$

$$(A_{12},B_{12},H_{12},E_{12},T_{12},D_{12})=\int_{-h_1/2}^{h_1/2}Q_{12}(1,z,z^2,z^3,z^4,z^6)dz,$$

$$(A_{22}, B_{22}, H_{22}, E_{22}, T_{22}, D_{22}) = \int_{-h_1/2}^{h_1/2} Q_{22}(1, z, z^2, z^3, z^4, z^6)dz,$$

$$(A_{44}, B_{44}, H_{44}, E_{44}, T_{44}, D_{44}) = \int_{-h_1/2}^{h_1/2} Q_{44}(1, z, z^2, z^3, z^4, z^6)dz,$$

$$(A_{66}, B_{66}, H_{66}, E_{66}, T_{66}, D_{66}) = \int_{-h_1/2}^{h_1/2} Q_{66}(1, z, z^2, z^3, z^4, z^6)dz,$$

$$r = \left(\frac{h_1}{8h_2} + \frac{h_3}{8h_2} - \frac{3}{4}\right),\ f_1 = \frac{3}{4h_2} G^{(c)}\bar{a} - \frac{9C_1}{4h_2} G^{(c)}\bar{b},\ \ f_2 = \frac{1}{2h_2} G^{(c)}\bar{a} - \frac{3C_1}{2h_2} G^{(c)}\bar{b},$$

$$f_3 = G^{(c)}\bar{a}r - 3C_1 G^{(c)}\bar{b}r,\ \ f_4 = \frac{3}{4h_2} G^{(c)}\bar{b} - \frac{9C_1}{4h_2} G^{(c)}\bar{d},\ f_5 = \frac{1}{2h_2} G^{(c)}\bar{b} - \frac{3C_1}{2h_2} G^{(c)}\bar{d},$$

$$f_6 = G^{(c)}\bar{b}r - 3C_1 G^{(c)}\bar{d}r\ ,\ \left(\bar{a}, \bar{b}, \bar{d}\right) = \int_{-h_2/2}^{h_2/2} (1, z^2, z^4)dz.$$

Author Contributions: **P. Roodgar Saffari:** Conceptualization, Data curation, Formal analysis, Project administration, Software, Investigation, Validation, Supervision, Writing - review & editing. **Sikiru Oluwarotimi Ismail:** Conceptualization, Formal analysis, Project administration, Software, Investigation, Validation, Supervision, Writing - review & editing, Writing—original draft. **C. Thongchom:** Conceptualization, Data curation, Formal analysis, Project administration, Visualization, Investigation, Validation, Supervision, Writing - review & editing. **S. Sirimontree:** Investigation, Data curation, Validation, Writing—original draft. **Thira Jearsiripongkul:** Investigation, Software, Validation, Formal analysis.

All authors have read and agreed to the published version of the manuscript.

Funding: This research received no external funding.

Institutional Review Board Statement: Not applicable.

Informed Consent Statement: Not applicable.

Data Availability Statement: Data sharing not applicable.

Acknowledgments: This study was supported by Thammasat Postdoctoral Fellowship, Thammasat University research Division, Thammasat University. Also, this research was supported by Thammasat University research Unit in Structural and Foundation Engineering, Thammasat University.

Conflicts of Interest: The authors declare no conflict of interest

References

[1] T.T. Soong, M.C. Costantinou, Passive and active structural vibration control in civil engineering, Springer, 2014.

[2] J. Tang, K.-W. Wang, Active-passive hybrid piezoelectric networks for vibration control: comparisons and improvement, Smart Mater. Struct. 10 (2001) 794.

[3] W.W. Clark, Vibration control with state-switched piezoelectric materials, J. Intell. Mater. Syst. Struct. 11 (2000) 263–271.

[4] R.T. Bonnecaze, J.F. Brady, Dynamic simulation of an electrorheological fluid, J. Chem. Phys. 96 (1992) 2183–2202.

[5] T. Hao, Electrorheological fluids, Adv. Mater. 13 (2001) 1847–1857.

[6] S. Kolekar, K. Venkatesh, J.-S. Oh, S.-B. Choi, Vibration controllability of sandwich structures with smart materials of electrorheological fluids and magnetorheological materials: a review, J. Vib. Eng. Technol. 7 (2019) 359–377.

[7] T.C. Halsey, Electrorheological fluids, Science (80-.). 258 (1992) 761–766.
[8] J.E. Stangroom, Electrorheological fluids, Phys. Technol. 14 (1983) 290.
[9] M. Ruzicka, Electrorheological fluids: modeling and mathematical theory, Springer, 2007.
[10] J.-Y. Yeh, L.-W. Chen, Vibration of a sandwich plate with a constrained layer and electrorheological fluid core, Compos. Struct. 65 (2004) 251–258.
[11] K. Wei, G. Meng, W. Zhang, S. Zhou, Vibration characteristics of rotating sandwich beams filled with electrorheological fluids, J. Intell. Mater. Syst. Struct. 18 (2007) 1165–1173.
[12] J.-Y. Yeh, Vibration and damping analysis of orthotropic cylindrical shells with electrorheological core layer, Aerosp. Sci. Technol. 15 (2011) 293–303.
[13] A.G. Arani, S.A. Jamali, H.B. Zarei, Differential quadrature method for vibration analysis of electro-rheological sandwich plate with CNT reinforced nanocomposite facesheets subjected to electric field, Compos. Struct. 180 (2017) 211–220.
[14] M.H. Gholamzadeh Babaki, M. Shakouri, Free and forced vibration of sandwich plates with electrorheological core and functionally graded face layers, Mech. Based Des. Struct. Mach. 49 (2021) 689–706.
[15] P. Shahali, H. Haddadpour, S. Shakhesi, Dynamic analysis of electrorheological fluid sandwich cylindrical shells with functionally graded face sheets using a semi-analytical approach, Compos. Struct. (2022) 115715.
[16] K. Khorshidi, B. Soltannia, M. Karimi, A. Ghorbani, Nonlinear vibration of electro-rheological sandwich plates, coupled to quiescent fluid, Ocean Eng. 271 (2023) 113730.
[17] N. Ghavidel, A. Alibeigloo, Free vibration analysis of cylindrical sandwich panel with electro-rheological core and FG-GPLRC facing sheets based on First order shear deformation theory referred by Qatu, J. Vib. Control. (2023) 10775463221148536.
[18] M.S. Dresselhaus, G. Dresselhaus, P.C. Eklund, A.M. Rao, Carbon nanotubes, in: Phys. Fullerene-Based Fullerene-Related Mater., Springer, 2000: pp. 331–379.
[19] H. Dai, Carbon nanotubes: opportunities and challenges, Surf. Sci. 500 (2002) 218–241.
[20] S. Iijima, T. Ichihashi, Single-shell carbon nanotubes of 1-nm diameter, Nature. 363 (1993) 603.
[21] C. Thongchom, P. Roodgar Saffari, P. Roudgar Saffari, N. Refahati, S. Sirimontree, S. Keawsawasvong, S. Titotto, Dynamic response of fluid-conveying hybrid smart carbon nanotubes considering slip boundary conditions under a moving nanoparticle, Mech. Adv. Mater. Struct. (2022) 1–14.
[22] T. Chang, J. Geng, X. Guo, Prediction of chirality-and size-dependent elastic properties of single-walled carbon nanotubes via a molecular mechanics model, Proc. R. Soc. A Math. Phys. Eng. Sci. 462 (2006) 2523–2540.
[23] E. Ghavanloo, S.A. Fazelzadeh, Vibration characteristics of single-walled carbon nanotubes based on an anisotropic elastic shell model including chirality effect, Appl. Math. Model. 36 (2012) 4988–5000.
[24] M. Strozzi, V. V Smirnov, F. Pellicano, M. Kovaleva, Nonlocal anisotropic elastic shell model for vibrations of double-walled carbon nanotubes under nonlinear van der Waals interaction forces, Int. J. Non. Linear. Mech. 146 (2022) 104172.
[25] P.K. Mallick, Fiber-reinforced composites: materials, manufacturing, and design, CRC press, 2007.
[26] S. V Joshi, L.T. Drzal, A.K. Mohanty, S. Arora, Are natural fiber composites environmentally superior to glass fiber reinforced composites?, Compos. Part A Appl. Sci. Manuf. 35 (2004) 371–376.
[27] X. Li, L.G. Tabil, S. Panigrahi, Chemical treatments of natural fiber for use in natural fiber-reinforced composites: a review, J. Polym. Environ. 15 (2007) 25–33.
[28] P.R. Saffari, S. Sirimontree, C. Thongchom, T. Jearsiripongkul, P.R. Saffari, S. Keawsawasvong, Effect of uniform and nonuniform temperature distributions on sound transmission loss of double-walled porous functionally graded magneto-electro-elastic sandwich plates with subsonic external flow, Int. J. Thermofluids. (2023) 100311.
[29] S. Sirimontree, C. Thongchom, P.R. Saffari, N. Refahati, P.R. Saffari, T. Jearsiripongkul, S. Keawsawasvong, Effects of thermal environment and external mean flow on sound transmission loss of sandwich functionally graded magneto-electro-elastic cylindrical

nanoshell, Eur. J. Mech. 97 (2023) 104774.
[30] C. Thongchom, P.R. Saffari, N. Refahati, P.R. Saffari, H. Pourbashash, S. Sirimontree, S. Keawsawasvong, An analytical study of sound transmission loss of functionally graded sandwich cylindrical nanoshell integrated with piezoelectric layers, Sci. Rep. 12 (2022) 1–16.
[31] C. Thongchom, T. Jearsiripongkul, N. Refahati, P. Roudgar Saffari, P. Roodgar Saffari, S. Sirimontree, S. Keawsawasvong, Sound transmission loss of a honeycomb sandwich cylindrical shell with functionally graded porous layers, Buildings. 12 (2022) 151.
[32] C. Thongchom, N. Refahati, P. Roodgar Saffari, P. Roudgar Saffari, M.N. Niyaraki, S. Sirimontree, S. Keawsawasvong, An experimental study on the effect of nanomaterials and fibers on the mechanical properties of polymer composites, Buildings. 12 (2021) 7.
[33] H.-S. Shen, Nonlinear bending of functionally graded carbon nanotube-reinforced composite plates in thermal environments, Compos. Struct. 91 (2009) 9–19.
[34] K.M. Liew, Z.X. Lei, L.W. Zhang, Mechanical analysis of functionally graded carbon nanotube reinforced composites: a review, Compos. Struct. 120 (2015) 90–97.
[35] P.T. Thang, T.-T. Nguyen, J. Lee, A new approach for nonlinear buckling analysis of imperfect functionally graded carbon nanotube-reinforced composite plates, Compos. Part B Eng. 127 (2017) 166–174.
[36] K. Mehar, S.K. Panda, A. Dehengia, V.R. Kar, Vibration analysis of functionally graded carbon nanotube reinforced composite plate in thermal environment, J. Sandw. Struct. Mater. 18 (2016) 151–173.
[37] R. Ansari, J. Torabi, M.F. Shojaei, Buckling and vibration analysis of embedded functionally graded carbon nanotube-reinforced composite annular sector plates under thermal loading, Compos. Part B Eng. 109 (2017) 197–213.
[38] T.N. Nguyen, C.H. Thai, H. Nguyen-Xuan, J. Lee, NURBS-based analyses of functionally graded carbon nanotube-reinforced composite shells, Compos. Struct. 203 (2018) 349–360.
[39] A.A. Daikh, M.S.A. Houari, M.O. Belarbi, S. Chakraverty, M.A. Eltaher, Analysis of axially temperature-dependent functionally graded carbon nanotube reinforced composite plates, Eng. Comput. (2021) 1–22.
[40] D.T. Huan, T.H. Quoc, V. Van Tham, C.T. Binh, Vibration Characteristics of Functionally Graded Carbon Nanotube-Reinforced Composite Plates Submerged in Fluid Medium, in: Mod. Mech. Appl., Springer, 2022: pp. 271–286.
[41] C.Q. Chen, Y. Shi, Y.S. Zhang, J. Zhu, Y.J. Yan, Size dependence of Young's modulus in ZnO nanowires., Phys. Rev. Lett. 96 (2006) 075505. https://doi.org/10.1103/PhysRevLett.96.075505.
[42] G. Stan, C. V Ciobanu, P.M. Parthangal, R.F. Cook, Diameter-Dependent Radial and Tangential Elastic Moduli of ZnO Nanowires, (2007). https://doi.org/10.1021/NL071986E.
[43] J. Hutchinson, N. Fleck, Strain gradient plasticity, Adv. Appl. Mech. 33 (1997) 295–361.
[44] H. Gao, Y. Huang, W.D. Nix, J. Hutchinson, Mechanism-based strain gradient plasticity—I. Theory, J. Mech. Phys. Solids. 47 (1999) 1239–1263.
[45] A.C. Eringen, Linear theory of nonlocal elasticity and dispersion of plane waves, Int. J. Eng. Sci. 10 (1972) 425–435. https://doi.org/10.1016/0020-7225(72)90050-X.
[46] A.C. Eringen, On differential equations of nonlocal elasticity and solutions of screw dislocation and surface waves, J. Appl. Phys. 54 (1983) 4703–4710. https://doi.org/10.1063/1.332803.
[47] M. Arefi, E.M.-R. Bidgoli, R. Dimitri, M. Bacciocchi, F. Tornabene, Nonlocal bending analysis of curved nanobeams reinforced by graphene nanoplatelets, Compos. Part B Eng. 166 (2019) 1–12.
[48] N.A. Fleck, J. Hutchinson, A phenomenological theory for strain gradient effects in plasticity, J. Mech. Phys. Solids. 41 (1993) 1825–1857.
[49] D.C.C. Lam, F. Yang, A.C.M. Chong, J. Wang, P. Tong, Experiments and theory in strain gradient elasticity, J. Mech. Phys. Solids. 51 (2003) 1477–1508. https://doi.org/10.1016/S0022-5096(03)00053-X.
[50] a. Jamalpoor, M. Hosseini, Biaxial buckling analysis of double-orthotropic microplate-systems including in-plane magnetic field based on strain gradient theory, Compos. Part B Eng. 75 (2015) 53–64. https://doi.org/10.1016/j.compositesb.2015.01.026.

[51] M. Hosseini, M. Bahreman, A. Jamalpoor, Using the modified strain gradient theory to investigate the size-dependent biaxial buckling analysis of an orthotropic multi-microplate system, Acta Mech. (2016). https://doi.org/10.1007/s00707-016-1570-0.
[52] A. Jamalpoor, A. Ahmadi-Savadkoohi, S. Hosseini-Hashemi, Free vibration and biaxial buckling analysis of magneto-electro-elastic microplate resting on visco-Pasternak substrate via modified strain gradient theory, Smart Mater. Struct. 25 (2016) 105035. https://doi.org/10.1088/0964-1726/25/10/105035.
[53] F. Yang, A.C.M. Chong, D.C.C. Lam, P. Tong, Couple stress based strain gradient theory for elasticity, Int. J. Solids Struct. 39 (2002) 2731–2743. https://doi.org/10.1016/S0020-7683(02)00152-X.
[54] S.K. Park, X.-L. Gao, Bernoulli–Euler beam model based on a modified couple stress theory, J. Micromechanics Microengineering. 16 (2006) 2355–2359. https://doi.org/10.1088/0960-1317/16/11/015.
[55] C.W. Lim, G. Zhang, J.N. Reddy, A higher-order nonlocal elasticity and strain gradient theory and its applications in wave propagation, J. Mech. Phys. Solids. 78 (2015) 298–313. https://doi.org/10.1016/j.jmps.2015.02.001.
[56] P. Roodgar Saffari, M. Fakhraie, M.A. Roudbari, Size-Dependent Vibration Problem of Two Vertically-Aligned Single-Walled Boron Nitride Nanotubes Conveying Fluid in Thermal Environment Via Nonlocal Strain Gradient Shell Model, J. Solid Mech. (2021).
[57] P. Roodgar Saffari, M. Fakhraie, M.A. Roudbari, Free vibration problem of fluid-conveying double-walled boron nitride nanotubes via nonlocal strain gradient theory in thermal environment, Mech. Based Des. Struct. Mach. (2020) 1–18.
[58] P.R. Saffari, M. Fakhraie, M.A. Roudbari, Nonlinear vibration of fluid conveying cantilever nanotube resting on visco-pasternak foundation using non-local strain gradient theory, Micro Nano Lett. 15 (2020) 181–186.
[59] R. Aghababaei, J.N. Reddy, Nonlocal third-order shear deformation plate theory with application to bending and vibration of plates, J. Sound Vib. 326 (2009) 277–289. https://doi.org/10.1016/J.JSV.2009.04.044.
[60] P. Phung-Van, Q.X. Lieu, H. Nguyen-Xuan, M. Abdel Wahab, Size-dependent isogeometric analysis of functionally graded carbon nanotube-reinforced composite nanoplates, Compos. Struct. 166 (2017) 120–135. https://doi.org/10.1016/J.COMPSTRUCT.2017.01.049.
[61] P. Phung-Van, C.-L. Thanh, H. Nguyen-Xuan, M. Abdel-Wahab, Nonlinear transient isogeometric analysis of FG-CNTRC nanoplates in thermal environments, Compos. Struct. 201 (2018) 882–892. https://doi.org/10.1016/J.COMPSTRUCT.2018.06.087.
[62] C.H. Thai, T.D. Tran, P. Phung-Van, A size-dependent moving Kriging meshfree model for deformation and free vibration analysis of functionally graded carbon nanotube-reinforced composite nanoplates, Eng. Anal. Bound. Elem. 115 (2020) 52–63.
[63] J.N. Reddy, A simple higher-order theory for laminated composite plates, (1984).
[64] M. Hosseini, A. Jamalpoor, Analytical Solution for Thermomechanical Vibration of Double-Viscoelastic Nanoplate-Systems Made of Functionally Graded Materials, J. Therm. Stress. 38 (2015) 1428–1456. https://doi.org/10.1080/01495739.2015.1073986.
[65] T. Murmu, S.C. Pradhan, Thermo-mechanical vibration of a single-walled carbon nanotube embedded in an elastic medium based on nonlocal elasticity theory, Comput. Mater. Sci. 46 (2009) 854–859.
[66] T. Murmu, S.C. Pradhan, Small-scale effect on the free in-plane vibration of nanoplates by nonlocal continuum model, Phys. E Low-Dimensional Syst. Nanostructures. 41 (2009) 1628–1633.
[67] P. Phung-Van, M. Abdel-Wahab, K.M. Liew, S.P.A. Bordas, H. Nguyen-Xuan, Isogeometric analysis of functionally graded carbon nanotube-reinforced composite plates using higher-order shear deformation theory, Compos. Struct. 123 (2015) 137–149.
[68] M. Hosseini, A. Jamalpoor, Analytical Solution for Thermomechanical Vibration of Double-Viscoelastic Nanoplate-Systems Made of Functionally Graded Materials, J. Therm. Stress. 38 (2015) 1428–1456. https://doi.org/10.1080/01495739.2015.1073986.
[69] S. Amir, Orthotropic patterns of visco-Pasternak foundation in nonlocal vibration of orthotropic graphene sheet under thermo-magnetic fields based on new first-order shear

deformation theory, Proc. Inst. Mech. Eng. Part L J. Mater. Des. Appl. 233 (2019) 197–208.
[70] N. Refahati, T. Jearsiripongkul, C. Thongchom, P.R. Saffari, P.R. Saffari, S. Keawsawasvong, Sound transmission loss of double-walled sandwich cross-ply layered magneto-electro-elastic plates under thermal environment, Sci. Rep. 12 (2022) 1–15.
[71] Y. Zarabimanesh, P. Roodgar Saffari, P. Roudgar Saffari, N. Refahati, Hygro-thermo-mechanical vibration of two vertically aligned single-walled boron nitride nanotubes conveying fluid, J. Vib. Control. 28 (2022) 2101–2120.
[72] L. Hadji, M. Avcar, Ö. Civalek, An analytical solution for the free vibration of FG nanoplates, J. Brazilian Soc. Mech. Sci. Eng. 43 (2021) 1–14.
[73] S. Ghahnavieh, S. Hosseini-Hashemi, K. Rajabi, A higher-order nonlocal strain gradient mass sensor based on vibrating heterogeneous magneto-electro-elastic nanoplate via third-order shear deformation theory, Eur. Phys. J. Plus. 133 (2018) 518.
[74] S.M. Hasheminejad, M. Maleki, Free vibration and forced harmonic response of an electrorheological fluid-filled sandwich plate, Smart Mater. Struct. 18 (2009) 55013.